NTNU

Norwegian University of
Science and Technology

A Method of Designing Wide Dispersion Waveguides Using Finite Element Analysis

Tom Alexander Solgård

Master of Science in Electronics
Submission date: July 2011
Supervisor: Peter Svensson, IET

Norwegian University of Science and Technology
Department of Electronics and Telecommunications

Problem Description

Controlled wide dispersion in loudspeakers is an important characteristic in the audio industry today. It is therefore desirable to investigate the use of a waveguide in order to control the dispersion from a direct radiating dome tweeter.

The project should assess existing solutions and study the adaptation of a waveguide (or alternative solutions for dispersion control) to a given tweeter. If possible, prototypes can be built and measurements of their performance can be compared with simulations.

Assignment given: 14. February 2011
Supervisor, NTNU: Peter Svensson
Supervisor, SEAS: Håvard Sollien

Abstract

High frequency dispersion has a great influence on the perceived performance of a loudspeaker. The directivity of a single transducer primarily depends on driver size, however directivity can be modified using an acoustical waveguide. A method of modelling and designing a wide dispersion waveguide for a loudspeaker soft dome tweeter has been developed.

A combination of finite element (FE) modelling and understanding of directivity and waveguides is used in order to prototype loudspeakers virtually. By utilizing computer simulations, the prototyping process is faster and more cost effective, all the while designing better performing loudspeakers.

Firstly, a baseline acoustic-structure interaction FE model of a tweeter was built in the COMSOL MULTIPHYSICS software. The model was verified by measurements, and the directional properties showed satisfactory agreement in the frequency range of interest. The accuracy of the baseline model allowed for credible simulations of waveguides.

Secondly, many waveguide geometry types were investigated, and a method for randomizing geometries and automating the design process was developed using the *Livelink for Matlab* module in COMSOL. Subsequently, a best fit waveguide design was selected based on a set of defined design criteria.

Thirdly, a prototype was built, the measured performance compared to the simulated model, and discrepancies investigated. The waveguide directivity performs as modelled through most of the working range, although deviations from simulations were larger than expected at frequencies above 12 kHz. The measurements validate the modelling procedure and emphasize the value of the design algorithm, even though the prediction accuracy may be improved. It can be shown that a waveguide of this type can, with only small modifications, be an effective way to increase HF dispersion for a large range of commercially available tweeters.

Acknowledgements

This Master Thesis is written as a result of a project equivalent to 30 ECTS credits required for the degree of *Master of Science* at the Norwegian University of Science and Technology (NTNU). The work was done at the Department of Electronics and Telecommunication under the Faculty of Information Technology, Mathematics and Electrical Engineering.

A number of people have contributed to this project. I want to thank Håvard Sollien at SEAS for enabling me to work on this interesting topic. He has been an invaluable help in the design process and by performing measurements. I would also like to thank my supervisor Peter Svensson for valuable feedback and guidance.

Master student Bjørn Kolbrek has contributed with his deep insight, knowledge and experience with loudspeakers. Our numerous and creative discussions have been a great help to me. Tim Cato Netland has kindly aided in the search for relevant literature.

Bertil Nistad and colleagues at COMSOL Support in Trondheim have enabled me to become proficient in advanced software with a high user threshold, in a short period of time.

Lastly, I want to thank SEAS and NTNU for providing the intellectual environment for the project.

Trondheim, July 3, 2011
Tom Alexander Solgård

Contents

Abbreviations

ALT	Acoustic Lens Technology
AOF	Aggregate Objective Function
BEM	Boundary Element Method
CAD	Computer Aided Design
CPU	Central Processing Unit
DOF	Degrees Of Freedom
EGO	Efficient Global Optimization
EMF	Electromotive Force
FE	Finite Element
FEA	Finite Element Analysis
FEM	Finite Element Method
FFT	Fast Fourier Transform
HF	High Frequency
LDV	Laser Doppler Vibrometer
LF	Low Frequency
LS	Loudspeaker
PA	Public Address
PDE	Partial Differential Equation
PML	Perfectly Matched Layer
RAM	Random Access Memory
SPL	Sound Pressure Level
WG	Waveguide

Chapter 1

Introduction

A method of modelling and automating the design of a wide dispersion waveguide for loudspeaker dome tweeters is presented in this thesis.

A prototype is built and the measured performance compared to the simulated model. The thesis combines Finite Element (FE) modelling and understanding of directivity and waveguides in order to prototype loudspeakers virtually. By utilizing computer simulations, the prototyping process is faster and more cost effective, all the while designing better performing loudspeakers.

This chapter gives an introduction to loudspeaker directivity and reviews some existing solutions.

1.1 Background

1.1.1 Loudspeaker directivity

Most loudspeakers today are conventional sealed or vented boxes, which are omnidirectional at low frequencies (LF) and forward directional at high frequencies (HF). The reason for this is that dispersion of direct radiators tend to diminish as the frequency increases. When wavelengths are long relative to the size of the radiator, the dispersion of energy tend to be omnidirectional. At short wavelengths the dispersion tends to be more directional. The dominant factor determining the beam width and its frequency dependence is the diameter of the radiating element in comparison to the wavelength of the radiated acoustic wave [1, 2]. In other words, the smaller the diameter of the radiating element in wavelength, the larger the angular beamwidth (the half-power (-3 dB) points of the main lobe).

Figures 1.1 and 1.2 illustrate this effect. This decrease in directivity is often referred to as *beaming*. The implication of this is that a transducer with flat amplitude response on-axis will have a significantly greater power output at LF compared to HF.

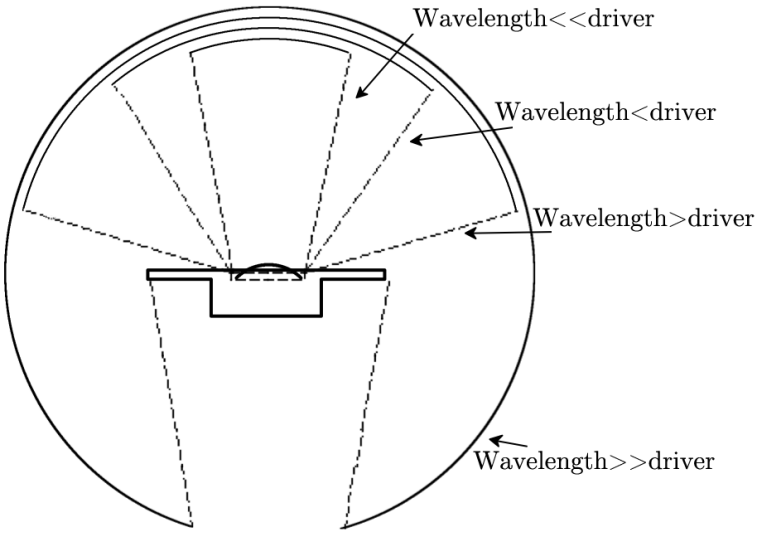

Figure 1.1: *Generalized dispersion of a direct radiator as a function of wavelength versus driver size (from [3]).*

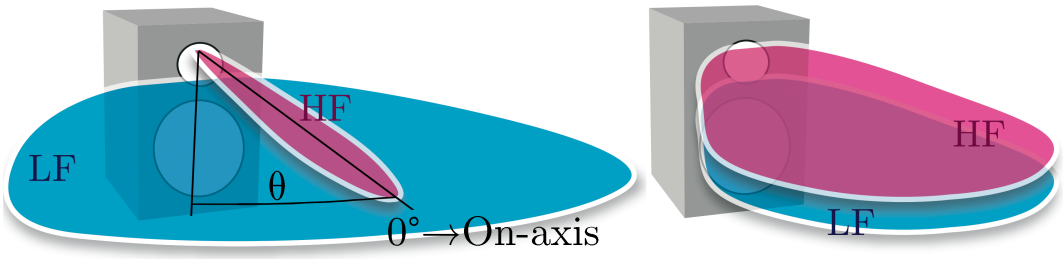

Figure 1.2: **Left:** *A conventional 2-way speaker dispersion pattern.* **Right:** *An ideal dispersion pattern. (from [4])*

Unfortunately, the acoustic energy of the radiation field is directly dependent upon the area of the radiating element for a given frequency and impedance [5]. Thus, the engineering of an acoustic transducer must consider a compromise between acoustic beam width and radiated acoustic

energy [1]. Beaming is especially critical at HF, as it is in this frequency range the most severe beam width collapse occurs. This results in spatial infidelity of the acoustic sound field [1], and listeners of the direct sound field in the peripheral region of a loudspeaker readily note this spectral aberration.

When the power output decreases with frequency, the loudspeaker will have deficient HF performance in reverberant rooms. Figure 1.3 depicts a typical listening situation in a room. The early reflections from walls, floor and ceiling will affect the perceived quality of the loudspeaker to a large extent. The early reflections usually have a substantial decrease in HF information, and the resulting sound can be perceived as "dull", "flat", "lifeless" etc.

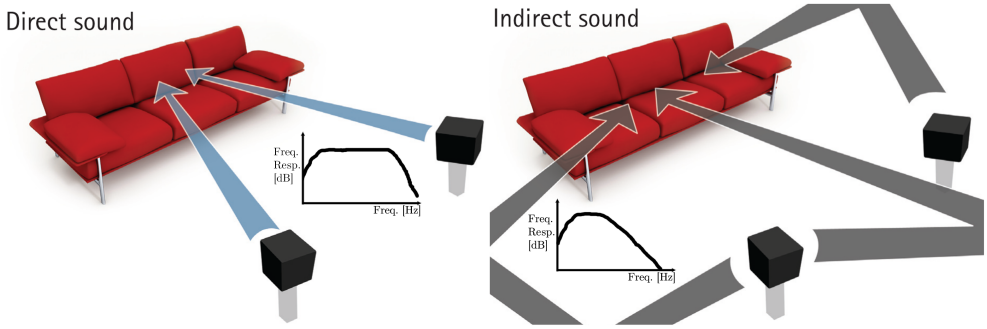

Figure 1.3: *Direct and indirect sound in a typical room. (from [4])*

Figure 1.4: Seas *27TFFC tweeter.*

Figure 1.5: Seas *27TBCD/GB-DXT.*

A loudspeaker is often comprised of several drivers, usually two or three. Each driver is responsible for reproducing a certain frequency range. The

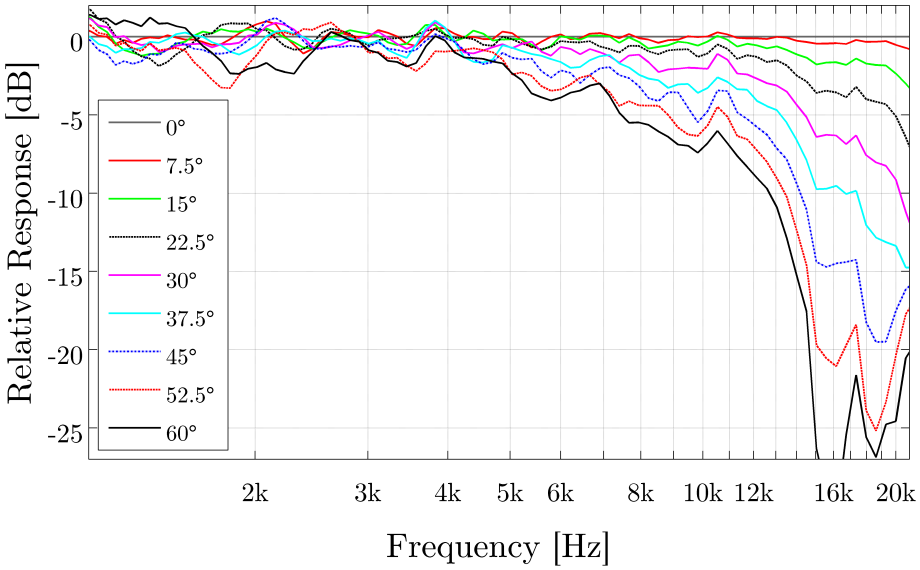

Figure 1.6: *Measured relative response (normalized to on-axis response) of 27TFF tweeter.*

transducer designed to produce HF (typically from 2-20 kHz) is referred to as a *tweeter*. The term *waveguide* will apply to any geometry added on to the baseline tweeter model throughout this thesis. Figure 1.5 shows a tweeter from SEAS with an example waveguide.

The goal of this thesis will be to find a solution to the beaming problem of the specific SEAS 27TFF soft dome tweeter shown in figure 1.4. Figure 1.6 shows the measured relative response of the tweeter at various angles, where 0° is the reference on-axis response. The relative response is the frequency response at a certain angle normalized to the frequency response at 0°. It is what the frequency response would look like if the loudspeaker were perfectly equalized flat on the axis. This way of visualizing directivity will be used throughout this thesis. Details of the measurement setup can be found in Section 3.1. The figure clearly shows the decay in HF reproduction as the angle increases.

The purpose of a waveguide is to control the dispersion characteristics of the sound source and it is often used to match the directivity of a HF transducer to the directivity of a LF transducer. Compared to a conventional tweeter, a successful waveguide design will have narrower dispersion at LF

and wider dispersion at HF in order to get smoother transitions between drivers. Manufacturers often use waveguides or reduced baffle sizes to reduce diffraction effects and to make dispersion more uniform and/or narrow.

1.1.2 Subjective loudspeaker preference

It is desirable to evaluate the subjective performance of a loudspeaker by objective measurements and criteria, and this section reviews some of the research on this topic.

It is often easy for a listener to differentiate between a reproduced recording on a set of loudspeakers and the "real thing" (for example being at a concert). The rendered soundscape is inherently unrealistic. The philosophy of achieving the most accurate reproduction is followed by prominent acousticians and loudspeaker designers like Siegfried Linkwitz [6], Sean Olive and Floyd E. Toole. Toole has done extensive work on evaluating the subjective performance of loudspeakers [7–11]. Findings show that a flat on-axis frequency response is preferred over inconsistent response and that a low level of nonlinear distortion is preferred over high levels.

Toole has also shown that loudspeakers with off-axis performance similar to on-axis are preferred over very directional loudspeakers in typical domestic living rooms [8, 9]. A smooth change in frequency response as the off-axis angle increases is preferred over abrupt changes. The reason for this is that the loudspeaker and room interaction is dependent on the loudspeaker directivity and that listening is frequently performed off-axis. Early reflections and diffuse reverberation are dependent on both the room acoustics and the off-axis response of the loudspeaker. Toole found that the precedence effect (important for localization) is more effective when the spectra of the direct and reflected sounds are comparable [12].

Olive [13] also found in a case study that the most preferred loudspeakers maintained the smoothest, flattest, and most extended frequency responses uniformly off-axis. He also found a model is that accurately predicts listener preference ratings of loudspeakers based on anechoic measurements [14, 15].

Queen [16] found that loudspeaker designs for home music listening rooms must consider directivity from the standpoint of uniformity of the intensity of arriving reflections with respect to frequency. He went on to specify loudspeaker design objectives of both a nondirectional horizontal radiation with restricted vertical dispersion, and a directional loudspeaker providing a uniform directional pattern with frequency [17].

When the directivity of the loudspeaker has a wide dispersion pattern over

a large frequency range, it will sound essentially the same in all directions in front of it. If the spectral stability of the HF content is independent of axial position, the monophonic real-source localization of the speaker is precise and unambiguous in all axial positions [1]. However, most loudspeakers have significantly degraded high-frequency response by the time the listener is more than 20° off-axis, which is a very typical listening condition. The source localization in this type of loudspeaker will be less accurate, and the loudspeaker will tend to disappear. Moulton [18] investigated phantom images in both stereophonic and monophonic music reproduction while testing a 360° horizontal dispersion loudspeaker system, and found that wide dispersion gave an enhanced sense of spaciousness, envelopment, and presence of performers, along with width and stability of phantom images.

The stereophonic quality of the playback will be better maintained off-axis if supported by the idealized off-axis high-frequency response. However, the time differences of arrival from the two loudspeakers will break down the stereo image as you move off-axis.

The binaural hearing mechanism contains directional and temporal masking effects that emphasize the importance of early sounds relative to later arriving ones [9]. Auditory cues for source direction, distance and surroundings are often corrupted by the loudspeakers, their placement and by room reflections. The influence of room reflections can be perceptually hidden from attention if reflections are sufficiently delayed (>6 ms) and attenuated [19]. When the direct and delayed reflected sound are added, constructive and destructive interference patterns occur depending on the amplitude and time delay of the addends. The reflections should have the same spectrum as the direct sound and the incidence of reflections relative to direct sound should be symmetric. A 3-dimensional phantom auditory scene can then be projected in front of the listener. Loudspeakers with constant directivity as a function of frequency (such as omni, dipole or cardioid), are necessary to determine spatial plausibility and believability of a stereophonic recording/mix [19, 20].

Timbre, localization and spaciousness are essential contributors to a satisfying auditory experience and should ideally be preserved from recording to reproduction. The loudspeakers should illuminate the room uniformly at all frequencies in order to somewhat remove the room behind the sound field [19]. A frequency independent polar response can be achieved with monopole and cardioid loudspeakers, although the directionality of a dipole is preferred as it reduces the excitation of room resonance modes while the figure-of-eight radiation pattern can be maintained down to the lowest

frequencies.

There should be a balance between the timbre of the direct sound and of the reverberant sound, based on the sum of the direct sound and the reverberant sound field being of similar magnitude at typical distances from loudspeaker to listening position [21].

A HF dispersion (at a -6 dB point) in conventional loudspeakers of $\pm 15°$ is generally considered to be acceptable, $\pm 30°$ to be good performance, while $\pm 45°$ is considered to be excellent [3]. A flat frequency response across a horizontal angle of 180° increases the *sweet spot* (the focal point between two speakers where a stereo mix is reproduced accurately) and yields benefits in terms of imaging, timbre and room interface [3].

A wide dispersion tweeter can be very useful in domestic HiFi and Home Cinema applications, as well as the automotive and professional audio industry. Home Cinema is a growing market [22], and wide dispersion insures that all listeners get the same experience. Normally, directivity control is not of great importance in studio monitors, but in some studios the mixing console where the recording engineer is working can be quite large. An extended sweet spot that would allow the engineer more freedom of movement would be very beneficial. A wide horizontal dispersion leads to a more constant timbre and uniformity in the area in front of the loudspeaker and enables the listener to move horizontally without a significant change in timbre [21].

There seems to be a trade-off between the directivity required to give the impression of being immersed in another acoustic space, and that required to preserve the illusion of compact sound sources in specifically localizable stereo images [9]. It is believed that strong early reflections from sidewalls are responsible for an enhanced sense of space, while maintaining adequate stereo image quality. Within concert hall design, the same trade-offs between early definition and spaciousness exist, although the delay time for these early reflections are much longer in a perceptual sense than in a typical home environment. Lateral early reflections have long been identified as providing a sense of envelopment and pleasant spatial sensations [23].

Toole [9] also believes that loudspeakers with good dispersion in the frontal hemisphere are preferable for domestic, recreational listening. Strong early reflections add an apparently pleasant sense of proximity to the original recording environment, while not appearing to be unduly detrimental to the quality of individually localizable stereo images. Hartmann [24] found that the early lateral reflections tend to delocalize the source, while the early floor

and ceiling reflections tend to reinforce the sense of localization. Listeners usually deem the sense of envelopment as being more important than the accuracy of sound source localization. Queen [17] confirmed the desirability of wide dispersing loudspeakers, given the preservation of uniformity of spectral energy. If the frequency responses at substantial angles off-axis are near parallel, the loudspeakers will exhibit smooth (but not necessarily flat) sound power responses and directivity indices [9].

Floor and ceiling reflections are in the same vertical plane as the direct sound, and these reflections are therefore likely only to result in comb filter effects, i.e. changes of the timbre. It was found in the EUREKA project *Archimedes* that the ceiling reflection and floor reflection contribute on individual basis to the timbre of a complete sound field in a typical listening room [25–28]. Walker [29] found that designing control rooms where the early reflections are delayed and/or attenuated (according to the *Archimedes* results) has proven to be advantageous in order to obtain a room independent sound impression irrespective of the general room characteristics.

Strong wall reflections from behind the loudspeaker are typically delayed by only a few milliseconds, which also result in comb filter effects, and should thus be avoided. An optimal design would therefore be a 180° wide dispersion pattern in the horizontal plane, while reducing vertical directivity. The result is that early lateral reflections from the loudspeaker to the listener have essentially the same frequency response as the direct sound, while HF content from reflections from the floor, ceiling, and wall behind the loudspeakers are constrained.

1.2 Design criteria

The main objective of this project is to find a way to achieve an improved directional performance for a given soft dome tweeter. The design criteria is presented in prioritized order as:

1. A smooth and flat relative response out to $45° - 60°$ off-axis
2. The possibility of correcting the on-axis response with a relatively simple passive filter/crossover design
3. A smooth and flat on-axis frequency response
4. Geometric size of waveguide/reflector should be practically small

5. Avoidance of possible production problems
6. Avoidance of geometries with higher probabilities of modelling error (tight geometries etc.)

Design criterion 2 is not essential if active filters are employed, but the necessity of active equalization limits the application areas and use of the modified tweeter.

1.3 Existing technology for dispersion expansion

SEAS have a tweeter model that aims to solve several well-known issues regarding directivity control, off-axis response and integration with mid-range units. This *27TBCD/GB-DXT* tweeter (from now on referred to as *DXT*) is shown in figure 1.5. It uses a licensed waveguide technology with concentric diffraction edges, which aims to expand the sound field at higher frequencies and increase directivity at LF.

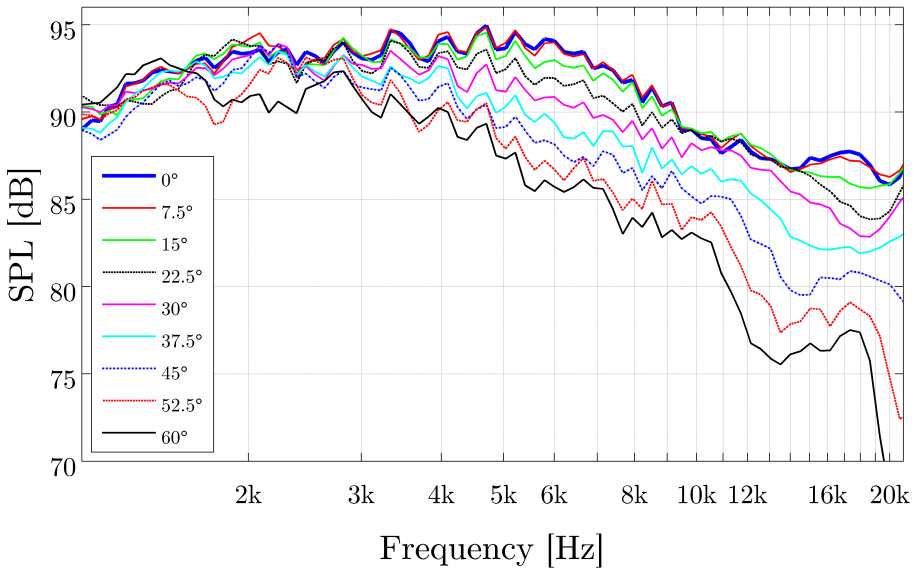

Figure 1.7: *Measured sensitivity of DXT tweeter*

DXT is an acronym for Diffraction eXpansion Technology and the patent [30] claims that the diffraction edges dampen the on-axis response

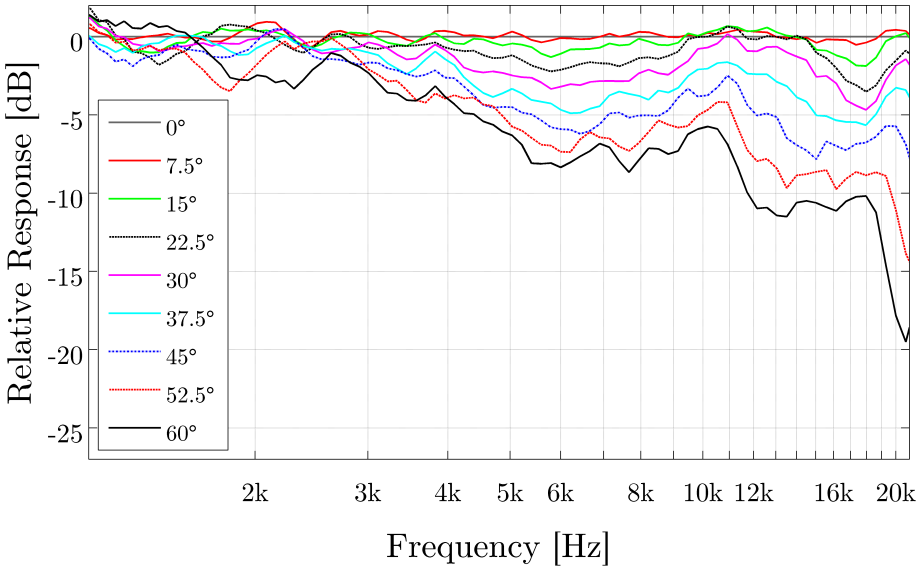

Figure 1.8: *Measured relative response of DXT tweeter*

while increasing the HF dispersion. The DXT brochure [4] states that the diffraction edges are effective from 7 kHz upwards and at HF the DXT uses up to third order diffraction to expand the sound field. Frequency response measurements of the DXT tweeter at angles up to 60° off-axis are presented in figure 1.7. Figure 1.8 shows the same measurements normalized to the on-axis response. This way of viewing the data gives better insight into the directional properties of the driver. Details of the measurement setup are given in Section 3.1.

The claims made of the DXT tweeter's directional performance seem to be somewhat backed by measurements, although there might exist other explanations for the performance than the ones stated in the patent and sales documentation for the tweeter. The driver specifications of the *27TBCD/GB-DXT* and *27TFCC* are listed in Appendix A.

Further investigation led to the discovery of a number of previous solutions to the problem of HF directivity. One example is the Acoustic Lens Technology (ALT) by Sausalito Audio shown in figure 1.9D. ALT is licensed to several loudspeaker companies, and the lens technology is used in the highly acclaimed Bang & Olufsen Beolab 5 loudspeaker (figure 1.9A) among others. Figures 1.10 and 1.11 present measurements (from a paper on ALT [3]), and show the improvement in directional properties introduced

Figure 1.9: **A:** *B&O Beolab 5* **B:** *Linkwitz Orion* **C:** *Linkwitz Pluto* **D:** *ALT* **E:** *PSB* **F:** *Spherex Xbox 5.1*

by the lens.

The ALT is based on the following design criteria [21]:

1. The power response should be as constant as possible given a flat on-axis free field sound pressure amplitude response
2. Avoidance of strong floor and/or ceiling reflections
3. Avoidance of strong reflection from the wall directly behind the loudspeaker

Figure 1.12 shows the relative frequency response of the B&O Beolab 5 at angles (from [21]). The reason for presenting this loudspeaker is that it is known to have one of the better directional properties on the market. The measurements (figure 1.12) show that the dispersion pattern is very wide and smooth across the entire audible range, as well as having a quite flat frequency response over a large bandwidth. Some verification of the ALT performance can be found in [31], and it appears to be a very successful implementation of their design goals. Moulton [1] states that use of the ALT lens to create a virtual source which displays exceptionally wide and frequency invariant vertical beam width and a 360° horizontal beam width,

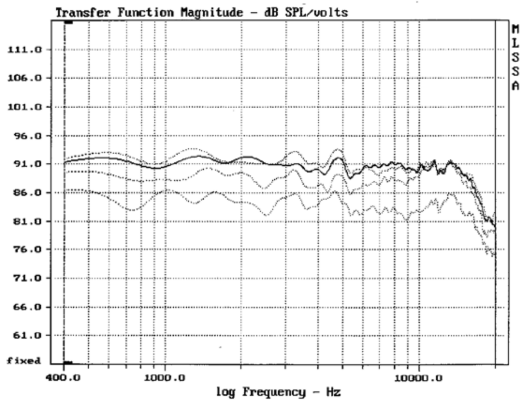

Figure 1.10: *Quasi-anechoic response of 3-way prototype at 0°, 30°, 60° and 90° off-axis using ALT lenses for midrange and tweeter sections. (from [3])*

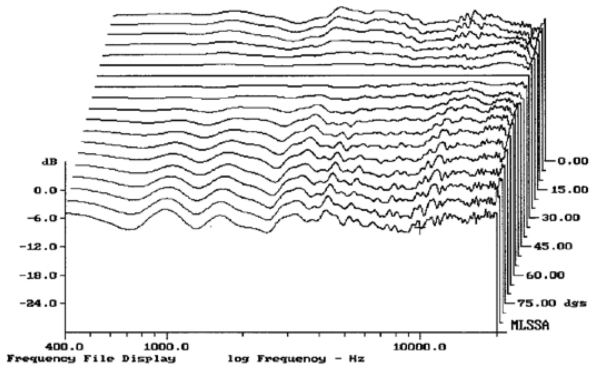

Figure 1.11: *"Polar Waterfall" of 3-way prototype using ALT lenses for midrange and tweeter. Normalized curves in 5° increments from* 0° *to 90° off-axis. (from [3])*

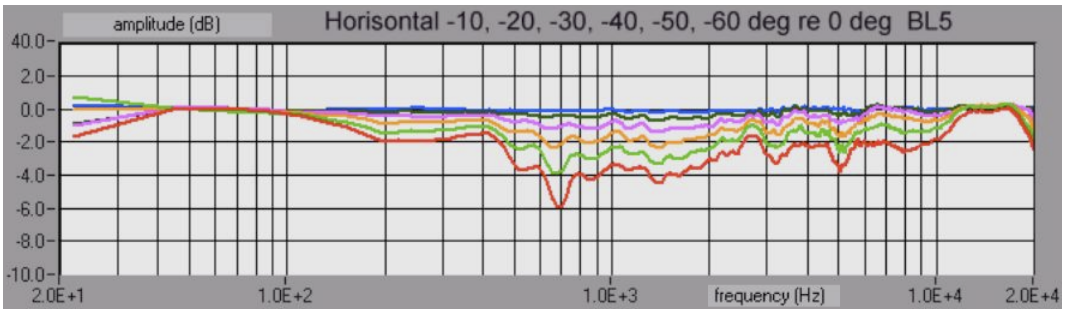

Figure 1.12: *Relative response at angles for B&O Beolab 5 (from [21])*

significantly enhances fidelity and image of the sound field.

Other loudspeakers that show seemingly well-performing directional properties are the bidirectional Linkwitz Lab Orion (figure 1.9B) and omnidirectional Pluto (figure 1.9C) [6]. Other companies using reflectors for increased HF dispersion in loudspeakers are Nacsound [32], Duevel [33] and Mirage [34]. Figures 1.9E & F show other examples of attempts to increase the dispersion at higher frequencies.

1.4 Virtual acoustic prototyping

This project will use the commercially available software COMSOL MULTIPHYSICS to model the acoustic-structure interaction in a tweeter with a waveguide. Finite Element Analysis (FEA) is useful because analytical solutions are not readily available for many of the geometries of interest. FEA has become the most generally used method for analyzing the physical behavior of structures with complex geometries, materials and boundary conditions, and has found uses in various aspects of loudspeaker design [35].

The method of virtual prototyping lowers the threshold for the engineer to try out new ideas and the advanced visualization tools allows for enhanced understanding. Use of FEA allows the designer to experiment with different mechano-acoustical structures without making expensive mistakes in terms of lead-time and tooling cost. Examples of studies that use FEA to further understand various aspects of direct-radiator loudspeaker systems can be found in publications such as [36–39]. FEA has found uses in various aspects of loudspeaker design, as can be seen in [35, 40–46].

Studies comparing numerical models with measured prototypes have previously achieved convincing and accurate results [35, 47–58].

Cobianchi [48] found that the directivity of a waveguide could be modelled accurately, and Salvatti [47] achieved excellent agreement for the prediction of beam-width as a function of frequency compared with measurements across a wide frequency range. His simulations were similar to measurements in the breakup region above 1 kHz, where the movement of the diaphragm is no longer pistonic. Jones [53] managed to accurately model the modes and breakups of a loudspeaker diaphragm. Henwood and Geaves [35] accurately and thoroughly modelled the modes of surround, spider and cone in an axisymmetric FE model of a woofer.

Optiz and Biba [59, 60] observed good agreement between measurements and simulations throughout the frequency range (100 Hz - 20 kHz) of a fluid-structure coupled analysis of a small headphone transducer. Anthony [61] is one of few to have modelled HF tweeters using FEA, and his simulations also show encouraging correlation to measurements up to 40 kHz.

Knowing the limitations of the models built and analyzed will be essential in the prototyping process. One purpose of this project is to get a better understanding of the physics of wave propagation, and the analysis should give insight for further development. Secondary effects such as the effects of

voice coil heating and nonlinear distortion can be neglected if small signal results are sufficient for the purpose at hand [47].

Further information on defining FEA models accurately can be found in [61–64].

1.5 Outline

This thesis is divided into six chapters, and an introduction to the problem is given previously. Key theoretical aspects needed to comprehend the text, like loudspeakers and the FE method, will be addressed in the second chapter.

A description of the establishment of a baseline model, and the development of a waveguide design algorithm are presented in chapter 3. Chapter 4 presents the results of the design process and compares simulations with measurements, before results are discussed in chapter 5. Finally, some concluding remarks are made in chapter 6.

Chapter 2

Theory

This chapter presents key theoretical aspects needed to comprehend this text. The reader is assumed to be knowledgeable in general acoustics and the workings of loudspeakers.

2.1 Loudspeakers

A general introduction to the functionality of loudspeakers can be found in the Loudspeaker Design Cookbook by Vance Dickason [65]. In the following, the focus will mainly be on the electromagnetic analysis of a loudspeaker driver, as this is the basis for the input to the FE model.

Modelling and simulation of the LF performance of loudspeakers by using lumped parameters is very well established [66–69], and computer simulation programs to assist designers and builders of loudspeaker systems are plentiful [70]. However, advanced simulation techniques such as FE modelling are needed to accurately predict the HF performance and breakup effects and model the underlying physical cause [36, 37, 71–73]. Lumped parameters models are not too useful in relation to the complex behavior and breakups of the diaphragm.

Some horn/waveguide geometries can be expressed analytically, but not necessarily for the given dome geometry. It is unlikely that any geometry we know the analytical solution of will render the wide dispersion sound field which we are interested in.

2.1.1 Electromagnetic analysis of loudspeakers

The following section presents an electromagnetic analysis of the current in the voice coil and the driving force that this current gives rise to. The equations following this derivation will be used in the acoustic-structure interaction analysis in COMSOL MULTIPHYSICS. The background for this derivation can be found in [47, 74].

One can calculate the force on a wire of length l, with the current I in a magnetic flux density B perpendicular to the wire, by the following equation:

$$F = I \cdot Bl \tag{2.1}$$

Bl is often known as the *force factor*, and is measured in tesla-meters [T·m]. Higher Bl values generate a larger force, given a constant current flowing through the voice coil.

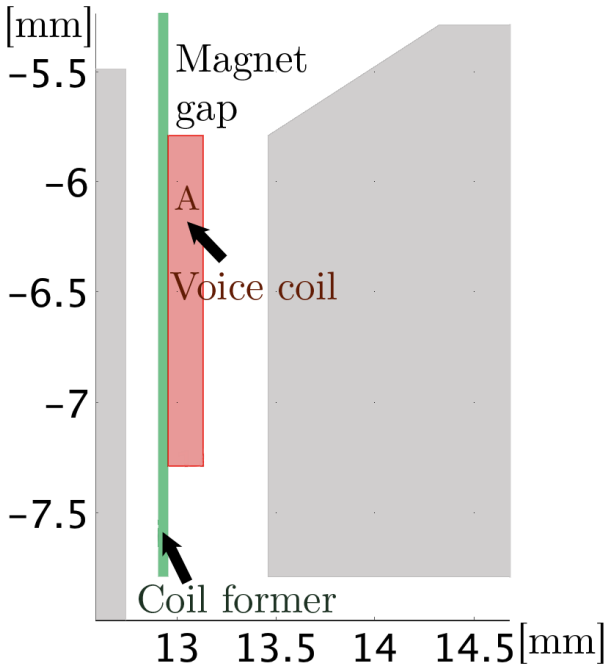

Figure 2.1: *Voice coil area A (red), coil former (green) and magnet gap*

The voice coil is wound in N turns of thin copper wire around a coil former, and occupies a cross-sectional area A (see figure 2.1). The total force F_e from the current on the coil can be expressed as an integral over the coil domain as

$$F_e = -I\frac{2\pi N}{A}\int r \cdot B_r \mathrm{d}A. \tag{2.2}$$

The current through the voice coil relates to the applied peak voltage V_0, the *blocked electric impedance* Z_b and the *back electromotive force (EMF)* $-V_{be}$, as

$$I = \frac{(V_0 + V_{be})}{Z_b}. \tag{2.3}$$

The blocked electric impedance is measured while the moving parts of the loudsspeaker are stationary, while the back EMF is the voltage that is induced in the coil as it moves through the permanent magnetic field in the gap.

If we consider the same coil in a magnetic flux density B, traveling at a velocity v perpendicular to the wire, we can evaluate the back EMF. An induced back EMF equal to $v \cdot Bl$ is induced in the wire, and total back EMF in the coil becomes

$$-V_{be} = -v\frac{2\pi N}{A}\int r \cdot B_r \mathrm{d}A. \tag{2.4}$$

If we combine equations 2.1 and 2.2, we can get an alternative expression for the force factor given as

$$Bl = -\frac{2\pi N}{A}\int r \cdot B_r \mathrm{d}A. \tag{2.5}$$

By combing equations 2.2 through 2.6, a usable expression for for the force applied to the coil can be obtained as

$$F_e = Bl \cdot \frac{V_0 - Bl \cdot v}{Z_b}. \tag{2.6}$$

The velocity of the moving coil is unknown prior to the acoustic-structure interaction computation. The force is applied, and a structural equation is solved in the moving parts of the driver, while a pressure acoustics equation is solved in the surrounding air domain. The coupling of physics is automatically assigned in Comsol. The pressure acoustic equation uses a *Normal Acceleration* boundary condition for the structural vibrations to propagate into the air domain, while at the same time the acoustic pressure is applied as a *Boundary Load* on the structure. These boundary conditions and their applications are further described in Section 3.2.

2.1.2 Coupling vibration to the air domain

By coupling the equations describing the structural vibrations and movement to the acoustic air domain, the resulting sound field can be described. This coupling is automatically done in COMSOL MULTIPHYSICS.

Another method of coupling structural vibrations to the air domain is by using the boundary element method (BEM) [75]. BEM is often more efficient than other methods like the FEM in terms of computational resources for problems where there is a small surface to volume ratio.

Often combined with BEM, the Rayleigh integral [76, 77] can be used to calculate the radiated field in an acoustic half-space if the normal displacement is known over the given radiating surface. In other words, the acoustic field surrounding a baffled vibrating panel is modelled by employing the Rayleigh integral, which directly relates the velocity potential (or sound pressure) in the acoustic domain to the velocity distribution on the plate [78].

However, the use of FEA is often chosen when dealing with multiphysics problems and when available computing power is sufficient.

2.1.3 Efficiency and sensitivity

The efficiency of a loudspeaker designates the amount of acoustic power and sound pressure level a loudspeaker can produce for each electrical watt of input power. It is defined as the sound pressure level generated with 1 W of input at a distance of 1 m. It is difficult to determine the true input power to a loudspeaker, as its impedance varies widely with frequency, both in magnitude and phase.

Modern solid-state amplifiers essentially operate as constant voltage sources as long as output stage current limits are not reached [79]. It is now common practice to specify loudspeaker performance in terms of voltage sensitivity. $2.83V_{rms}$ ($4V_{peak}$) represents the voltage that will produce 1 W of power dissipation in an 8 Ω resistor.

2.2 Finite Element Method

Some simple waveguide/horn expansions can be solved analytically with a few assumptions [80, 81]. However, as the geometry increases in complexity, analytical solutions become cumbersome at best. In these situations, approximate numerical methods must be must be applied.

In the Finite Element Method (FEM), the geometry is divided into discrete elements, which when combined form a *mesh*. Differential equations

describing the physical problem are solved by numerical methods at the nodes of the mesh. Linear stress-strain equations are used in the mechanical domain (works for small deformations), while the Helmholtz wave equation is used in the acoustic domain.

FEM is benefitial to use when

- the domain is complicated or moving.
- the mesh is irregular through the domain.
- the needed precision varies inside the domain .
- you want to model diffraction.
- you need to remesh between time steps.

The accuracy of the solution is based on the validity of the assumption that pressure variations are small and linear. The nonlinear behavior of air at high SPL's and effects of viscous damping in small cavities are not modelled [50].

2.2.1 Element size

We know from the Nyquist theorem that the mesh needs to resolve the wavelength by at least two elements per wavelength, for the solution to have any meaning at all [82]. However, such a coarse grid is useless in practice. As well as resolving the shortest wavelength, the geometrical details of the model must be resolved. Most often fine geometrical details become interesting only when their size is comparable to the wavelength of interest.

There seems to be some debate on how many elements should resolve each wavelength. Some claim that the maximum element size should be smaller than one-sixth of the wavelength of the acoustical wave [83]. Some have found that 4 elements per wavelength suffice in order to obtain an accurate solution [47,48]. The number of elements needed are also dependent on type of element (be it triangular, quadrilateral etc.) [84].

The geometry in this thesis is meshed with a Free Triangular Mesh with a maximum element size of

$$l_{max} = \frac{c_{sound}}{f_{max}} \cdot \frac{1}{6}[m] \tag{2.7}$$

where c_{sound} is the speed of sound in air and f_{max} is the maximum frequency to be studied accurately.

2.2.2 Material properties

Obtaining useful results depend on having accurate material parameters for every part of the driver. Reliable material data is rather to hard find, as most of the material databases found online and in the COMSOL material library are limited. Stated properties can often differ from the actual values by a factor of 2 or 3, which makes them almost useless for predictive simulations [47].

Material damping is the loss of energy occurring through motion of a structure. It is a physical process that has several causes, which are difficult to express mathematically [35]. In a composite structure such as a loudspeaker the different materials involved will each have their own distinct damping.

The damping is commonly specified by a hysteretic model [35], where Young's modulus is complex; E is the standard Young's modulus, and η is a damping loss factor. In the frequency domain the complex numbers indicate a difference in phase. Both E and η will in general vary with frequency, although not in an easily predictable way.

Materials commonly used in transducers often exhibit frequency dependent properties, and this should ideally be accounted for in the simulation. Parameter values are usually temperature sensitive, and vary with frequency and the amplitude of the applied force. The normal approach is to ignore the nonlinearity and adjust the parameters to be used in the simulated model so that it agrees well with measurements obtained from commonly available commercial equipment.

Anisotropic or otherwise inhomogeneous materials (such as variations in chemical treatments or material densities within the components) can be present and be a potential accuracy problem. Accurate material measurements of the elastic modulus, density, and damping are essential if useful predictive engineering models are desired [47].

Methods for measuring material properties are widely covered in available publications and ASTM standards [47]. Extensive and accurate material parameter values cannot normally be obtained without considerable cost [35].

The geometry and density are usually quite straightforward to measure. Henwood and Geaves [35] describe a way to use a laser Doppler vibrometer (LDV) and electrical impedance measurements to determine a reasonable estimate of Young's modulus, E, and the damping properties. By comparing the amplitudes of the early modes and their frequencies, the material E can

be adjusted accordingly. The cone damping can be estimated through the general impedance, although with some increased difficulty. Jones [53] also applied damping by using a complex Young's modulus with a material loss factor in the stiffness matrix.

Hedges [52] implemented a way of using frequency dependent material parameters by defining a loss factor function in COMSOL. As the parameters are not published in the relevant frequency range, he approximated the damping factor as a function of frequency by matching the amplitudes of modes in a driver model with measurements, much like the method described by Henwood and Geaves.

Experimental data for the variation of material properties with frequency is rarely available, and if it were, its use would reduce the calculation efficiency. The material properties are usually assumed to be constant (as they are in the current work), and will not necessarily prevent a good agreement with measured values.

A thorough study of the material properties of the moving parts used in the tweeter simulation is beyond the scope of this project.

Chapter 3

Modelling Method

This chapter firstly describes the measurement setup, followed by a description of the modelling process of a baseline tweeter. A method of automating the design process of a waveguide is subsequently presented, before finally the best performing geometry is selected for prototype development.

3.1 Measurement setup

Most of the measurements were performed by Seas in their anechoic chamber. It consists of a shell of concrete and Leca that rests on coil springs to dampen vibrational noise from the ground. The mass of the concrete shell ($\approx$ 200 tons) and springs results in a 2nd order low pass filter with a cut off frequency of 3 Hz. The dimensions inside the shell is (L x W x H) 960 cm x 650 cm x 755 cm. The walls, floor and ceiling are covered with mineral wool wedges placed 5cm from the walls, resulting in an absorption coefficient of more than 0.99 for frequencies above 70 Hz. The floor is a net made from tensioned steel wires [85].

The tweeter was put in a baffle with dimensions of 80cm x 60cm and measured at 1 m distance (see figure 3.1). The tweeter is placed off center (as seen in the figure) to evenly disperse the edge diffractions. The ratio of distances to each edge is about 1.33. The baffle size is chosen so that it is practical and manageable, and that the dipole cancellations are too low in frequency to significantly affect the measurements in the working range of the tweeter. The measurements are performed using a logarithmic sweep in the range 200 Hz - 40 kHz at $2.83V_{rms}$. A rectangular window of 70 ms is applied to the impulse responses and a $^1/_{24}$ octave band smoothing to the

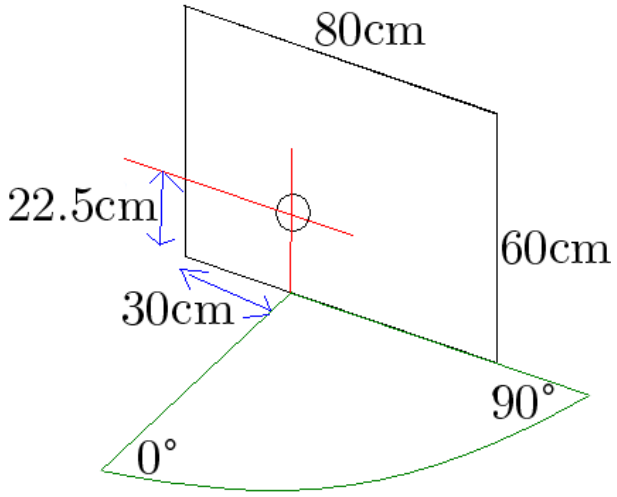

Figure 3.1: *Measurement setup dimensions of tweeter placed in baffle.*

frequency responses. The following equipment is utilized in the measurement setup:

- Klippel Distortion Analyzer 2
- PC with Klippel dB-lab 202.52 software (TRF-module)
- Microphone: B&K Type 4133
- Microphone preamp: B&K Type 2639
- Microphone preamp: G.R.A.S. Power Module Type 12AK
- Microphone calibrator: B&K Sound Level Calibrator Type 4230
- Amplifier: Lab.gruppen iP 2100

3.2 Establishing a baseline model

Comsol Multiphysics version 4.1 is the commercial software package used for the FEA. The Acoustics Module is an add-on package that contains built-in application modes and boundary settings for acoustic propagation in solids and stationary fluids. Comsol offers an extensive Livelink interface to Matlab and CAD software, is cross-platform and flexible in programming, pre- and post-processing.

3.2.1 Building the model and defining the physics

The geometry was created in a 3D CAD environment, of which an accurate 2D slice was imported into Comsol. The slice was slightly tuned to be able to attribute physical properties to the model. A Comsol tutorial model of a loudspeaker woofer [74] was used as a starting point, and substantially modified to suit the needs of this project. The model is largely based on the work of Jones [53]. The tweeter to be modelled is presented in figure 3.2, 3.3 and 3.5.

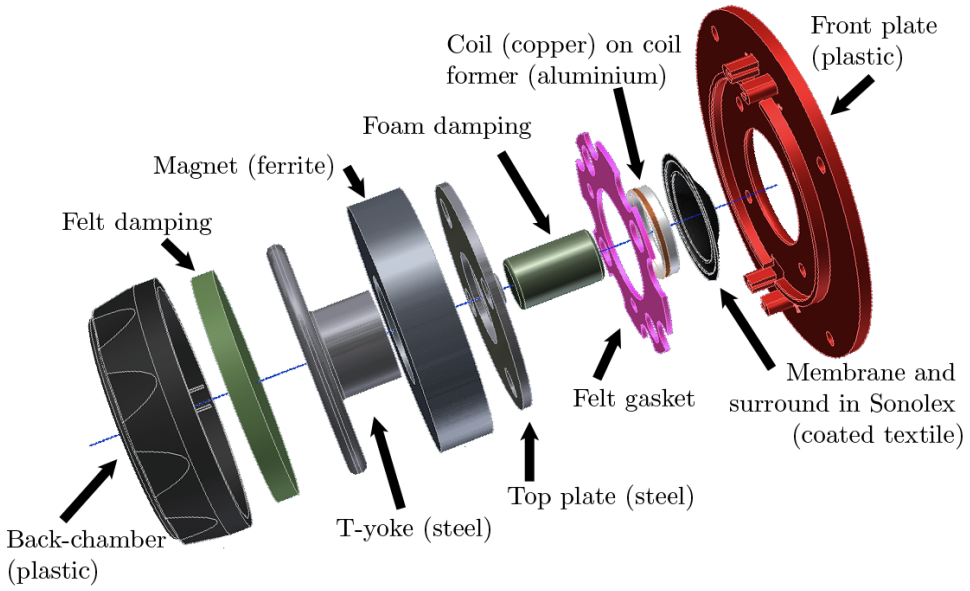

Figure 3.2: *Parts and materials of 27TFFC tweeter*

The material data are taken from Comsol material database and driver information from Seas (Appendix A) and can be seen in table 3.1. The real and imaginary parts of the blocked coil impedance as a function of frequency are imported, linearly interpolated and defined as variables, so that they are available for any specified frequencies. The driving force applied to the coil can then be calculated as given in eq. 2.6.

The Acoustic-Structure Interaction Module is used to model the physics in Comsol. The bidirectional physical coupling is done automatically when

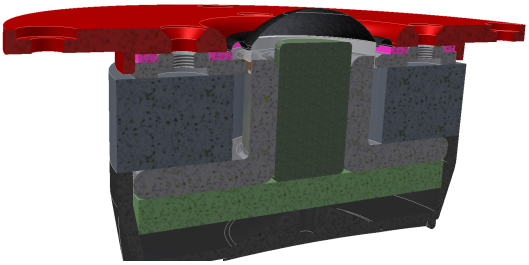

Figure 3.3: *27TFFC tweeter cut plane*

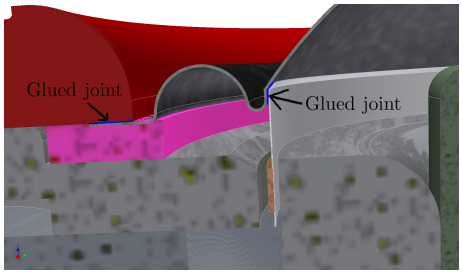

Figure 3.4: *Glued joints on 27TFFC*

	Diaphragm/Surr. (Sonolex textile)	Coil-former (aluminum)	Voice coil (copper)	Glue
Young's mod. [MPa]	1500	75000	150000	1290
Poissons's ratio	0,33	0,33	0,33	0,4
Density [g/cm^3]	0,894	2,883	5,331	0,6
Weight [g]	0,132	0,057	0,131	—
Isotropic Loss Factor	1.1			

Table 3.1: *Material data*

boundaries are assigned the correct attributes and the *Acoustic-Structure Boundary* is specified. These attributes are presented in the following.

The *Axial Symmetry boundaries* are defined as shown in figure 3.7. *Initial Values* are needed to solve the set of equations and are set to zero across the domains.

Within the *Pressure Acoustics* physics sub-node in Comsol, the attributes mentioned in the following must be defined. The *Sound Hard Boundary (Wall)* condition is applied to all rigid parts, which are assumed to be completely reflective surfaces.

Comsol contains an intrinsic far field capability similarly as in BEM, and measurement points were defined for the far field SPL at 1 m in intervals of 7.5° from 0° to 60° (the largest angle of interest). The *Far-Field Calculation* condition is set to the boundary shown in figure 3.6. Utilizing the full Helmholtz-Kirchhoff integral allows us to calculate the pressure at any point at a finite distance from the source surface [86]. The acoustic center is placed centered in line with the baffle.

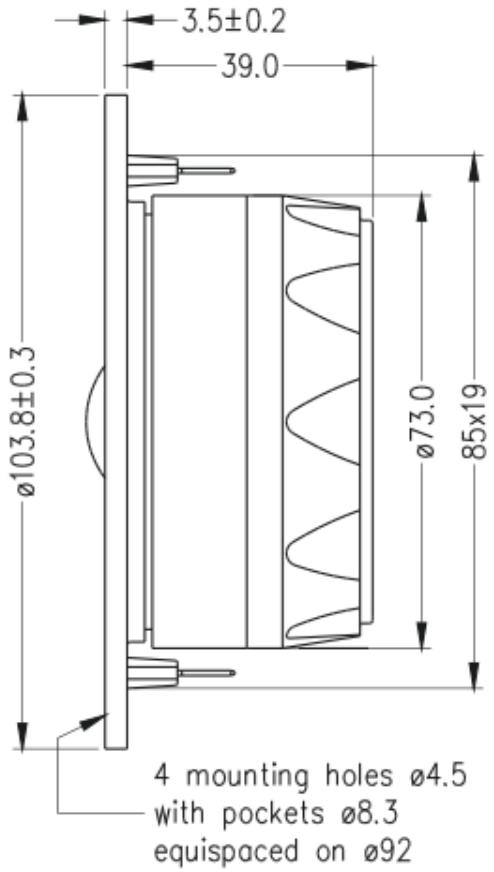

Figure 3.5: *27TFFC dimensions*

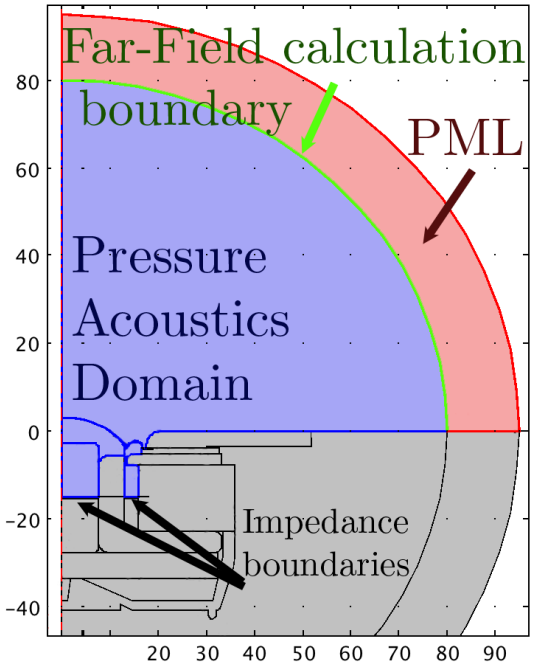

Figure 3.6: Pressure Acoustics *domain (in blue)*, PML *(in red)*, Far-Field Calculation *boundary (in green)* and Impedance *boundaries (in* **black***)*.

The Perfectly Matched Layer (PML) is marked in red (in figure 3.6), and simulates an infinite domain. The PML is needed to create a domain boundary without reflections. It is an artificial absorbing layer for waves, used here to truncate the computational region in order to simulate a problem with open boundaries. It is stated to work for any incident angle of sound waves [86]. A more theoretical review of PML can be found in [84]. A simpler boundary condition called the *Spherical Wave Radiation* can be used in situations where the waves out of the domain are assumed to be spherical, emanating from a given point in space.

When the *Impedance Boundary Condition* is set set to the impedance of air ($1.2[kg/m^3]\cdot 343[m/s]$), it absorbs any incoming plane wave completely. This boundary condition is used to avoid resonances in the back chamber and in the chamber behind the magnet gap (shown in figure 3.6). The

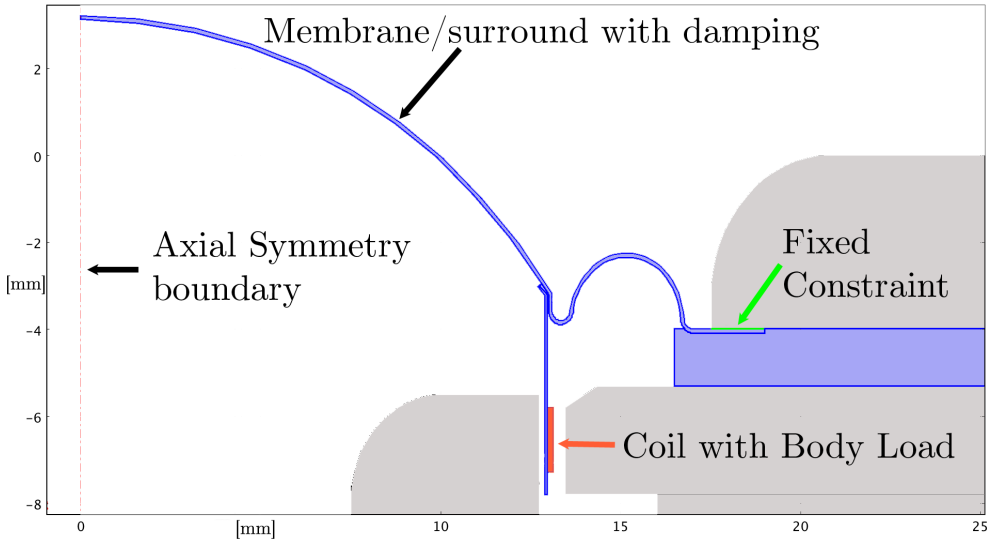

Figure 3.7: Linear Elastic Model *domain (blue). The voice coil has a* Boundary Load *condition (red) in the upwards direction and a* Fixed Constraint *on the boundary (green) where the diaphragm is glued to the front plate.*

resonance in the magnet chamber at 6 kHz is clearly seen in figure 3.8 and 1/4 wavelength matches the depth of the chamber (14.5 mm). The real tweeter has foam damping in the back chamber and ferrofluid (magnetic oil) in the magnet gap, which effectively dampens these resonances.

Within the *Linear Elastic Material Model* sub-node COMSOL, the attributes mentioned in the following must be defined. All moving parts are defined with the *Free* condition (allows the parts to move freely), while the boundary where the diaphragm is glued to the front plate (as seen in figure 3.4 and 3.7) is set to a *Fixed Constraint* condition. In order for the *Linear Elastic Material Model* to be an accurate representation of the the driver movement, the structural deformations should be small, as is the case in this model.

An *Isotropic Loss Factor* type *Damping* is applied to the diaphragm/surround with the Sonolex material. The loss factor η is a measure of the inherent damping in a material when it is dynamically loaded. The value was manually tuned ($\eta = 1.1$) so that the driver sensitivity would closely match on-axis measurements.

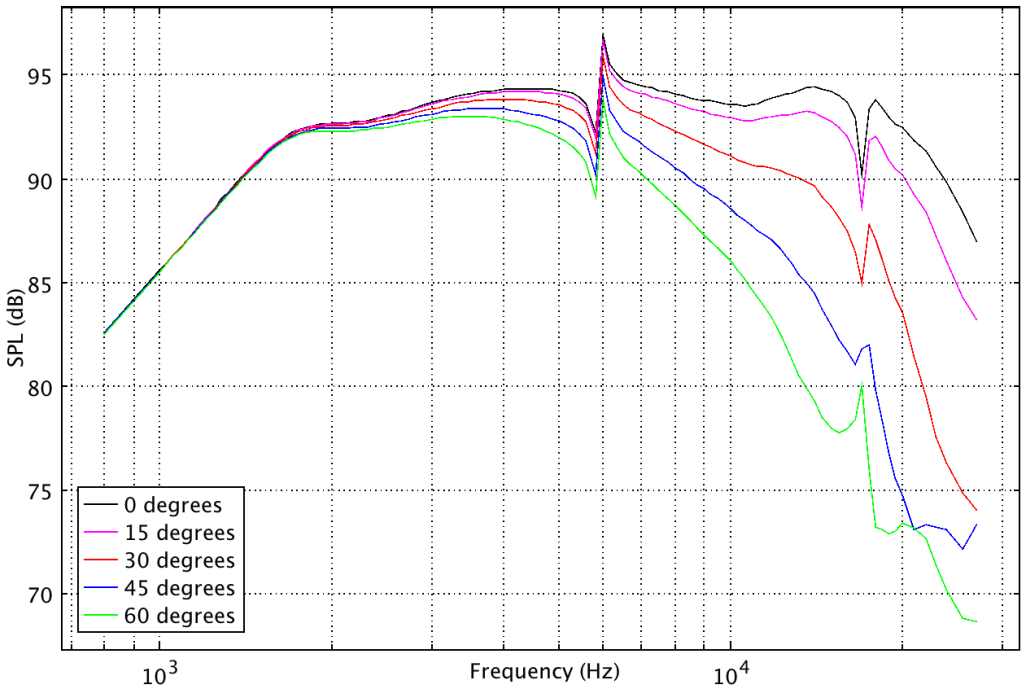

Figure 3.8: *Modelled sensitivity of tweeter without damping in the magnet chamber. Note the resonance at 6 kHz.*

A *Body Load* is applied to the voice coil as shown in figure 3.7. The force is defined from equation 2.6 and works upwards, parallel to the axis of symmetry.

After the discussed physical properties have been defined, a frequency domain study can be performed. A frequency sweep with 30 frequencies logarithmically spaced from 1.25-20 kHz is executed for each geometry. Time domain results can be obtained by solving the model over a range of frequencies and performing an inverse Fourier transform [84]. However, no such post-processing to the time domain has been performed in this project.

An advantage of using the *Acoustic-Structure Interaction Module* is the ability to model the moving diaphragm much more accurately than by defining a surface as a perfect piston. Breakups and out-of-phase movements as shown in figure 3.9 are included in the model.

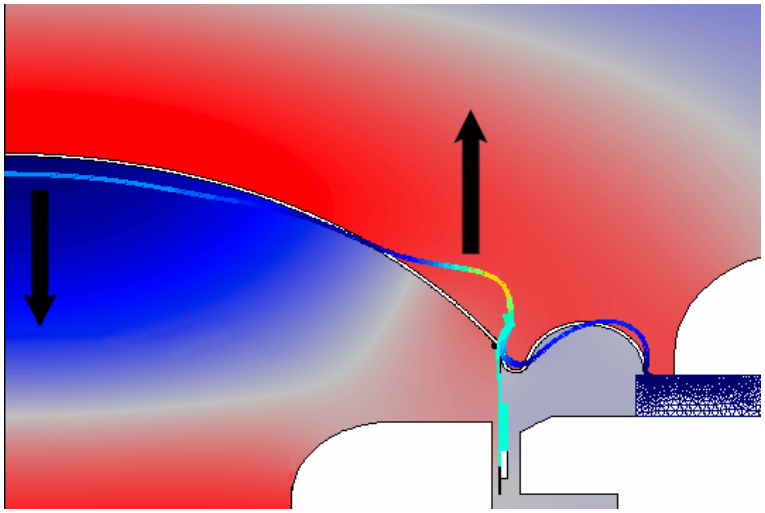

Figure 3.9: *Displacement of diaphragm (upscaled). The arrows show parts of the diaphragm out of phase.*

3.2.2 Meshing

Both the meshing of the moving parts in the mechanical domain and the air in the acoustic domain need to be considered. Hedges [52] studied the effect of mesh resolution in narrow regions and found that this parameter has little effect on the final result of the model. The findings correspond to the experiences from this project. Increasing the mesh resolution of narrow regions by four times the default value did not affect the resulting solution. Consequently, a resolution of 1 element per width of the diaphragm is sufficient (see figure 3.10). This will help keep the model computationally effective, while preserving accuracy. Note that the somewhat coarse meshing excludes modelling of the insides of the diaphragm, but this is a viable assumption for the thin diaphragm.

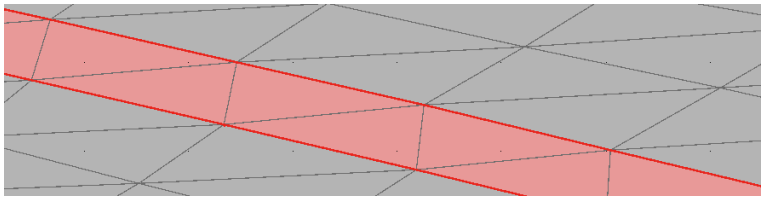

Figure 3.10: *Acceptable mesh resolution in narrow region (diaphragm in red).*

Kyouno [87] found that the acoustic load on the diaphragm is of great importance in a vibro-acoustic coupling in a model of a compression driver and horn. Hedges [52] also found that to properly model the mass of the air load on the cone, the radius of the sphere containing air in front of the driver must be greater than four times the radius of the cone. The air domain in the model has a radius of 80 mm, which is more than four times the diaphragm radius of 17 mm (and thus meeting the criteria for accuracy).

3.3 Preliminary waveguide study

After the baseline model was verified and deemed sufficiently accurate, a range of different waveguide geometries was simulated. Initially, a general geometric parametrization was made where many line segments could be changed to model any expansion or flare rate between two points. The outer point was set to a typical waveguide size, comparable to the DXT (height 14 mm, radius 52 mm). Some of the geometries modelled in this parameterization are shown in figure 3.11.

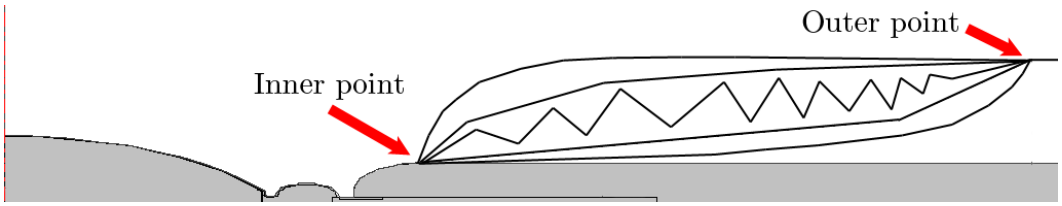

Figure 3.11: *Initial parameterization of typical waveguide geometries between two points*

A MATLAB script was written to generate geometries and a parametric sweep of waveguide geometries was performed in COMSOL. Concave and convex geometries, different exponential expansions and more obscure forms of waveguides were studied, and it quickly became apparent that neither of the geometries within these boundaries would achieve the design goals set in Section 1.2. A natural next step was therefore to broaden the search range and to explore other options. Figure 3.13 shows a number of the tested waveguide and acoustic reflector geometries.

A fellow student directed the author's attention to a patent by Wente [88] (see figure 3.12). The patent sought to diminish the directive character of frequencies above 5 kHz. A geometry similar to this was tested, and is

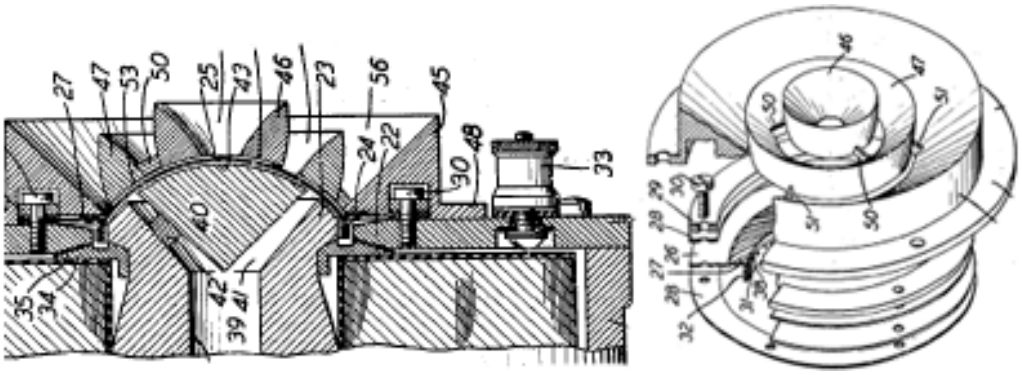

Figure 3.12: *US patent* 1930915 *by E.C. Wente, 1933*

shown in figure 3.13H.

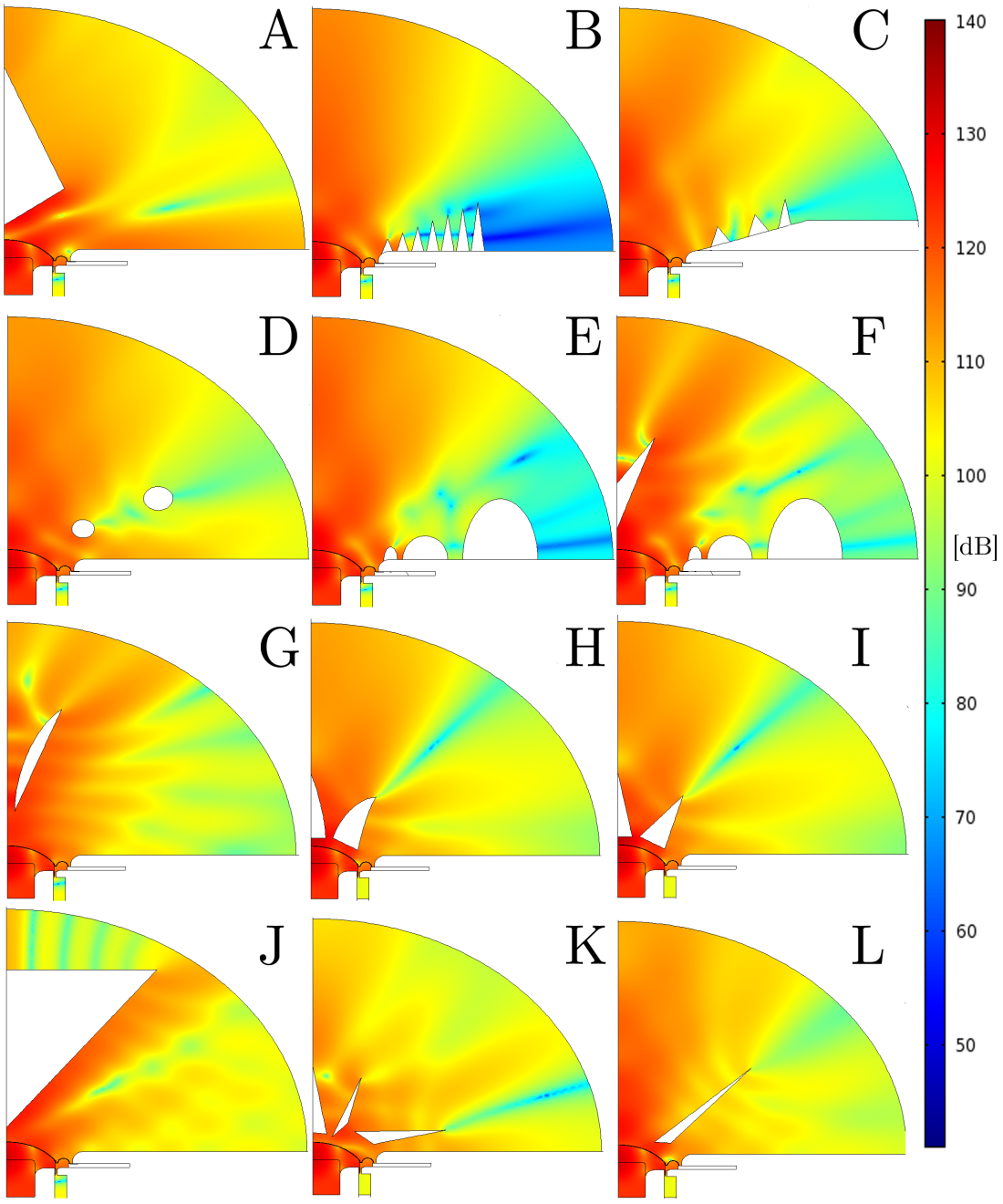

Figure 3.13: *Some of the simulated types of waveguide and acoustic reflector geometries (SPL@20 kHz).*

3.4 Parameterizing and randomizing waveguide geometry

The preliminary testing of different waveguides gave some indication to what geometries could be useful. A waveguide such as the one in figure 3.13H showed promising flat directivity properties up to 10 kHz and was chosen for further study. By varying this geometry, one could hope to improve the response at higher frequencies. By making the waveguide conical as seen in figure 3.13I, geometric parameterization could be implemented easily. The performance difference between the curved cones and the conical ones proved to be minimal.

As the correlation between response and geometry is hidden (it is difficult to give an intuitive relation between performance and geometry), an algorithm that iteratively changes the geometry towards better performance is hard to find. The many degrees of freedom in the geometry do not simplify the situation, and a target function describing the desired response is nontrivial as well (see Sections 3.4.1 and 3.4.2).

Optimizing the geometry gradually by hand would indeed be an arduous process. Fortunately, COMSOL can be controlled and run through other programming languages such as Java and MATLAB. COMSOL is run as a server and is accessible in MATLAB through the LiveLink API [89]. The specially written MATLAB scripts can be found on the appended DVD (Appendix C). The vertices of the waveguide geometry was parameterized and given ranges as shown in figure 3.14. The script randomizes the vertices within the given range and performs checks if the resulting geometry is valid (avoids inverted geometries). The ranges are set so that the resulting geometry is possible to fabricate in practice.

The script continues to run the altered COMSOL model, retrieves the data and saves the results so that they are available for post processing. The biggest advantage of the script is that it can run several hundred geometries overnight without supervision. As the geometries are randomized, we cannot be sure that the best geometry is represented within the sample space. However, by running hundreds of geometries the chance of getting some geometry quite close to the optimum is high. Alternatively, the vertices could be swept through the geometric ranges in a deterministic fashion.

A combined plot with sensitivity, relative response and the corresponding geometry was output by the MATLAB script for each simulated waveguide.

This allowed for effective visual screening of each geometric sweep, and a selection of the best performing waveguides could be made.

The geometric range of the vertices can be reduced when a promising geometry has been found, and in this iterative way optimize it further. Figure 3.14 shows the reduction of the geometric search ranges through several stages in the iteration process. An edited and shortened example script of the last geometric iteration stage is presented in text in Appendix B.

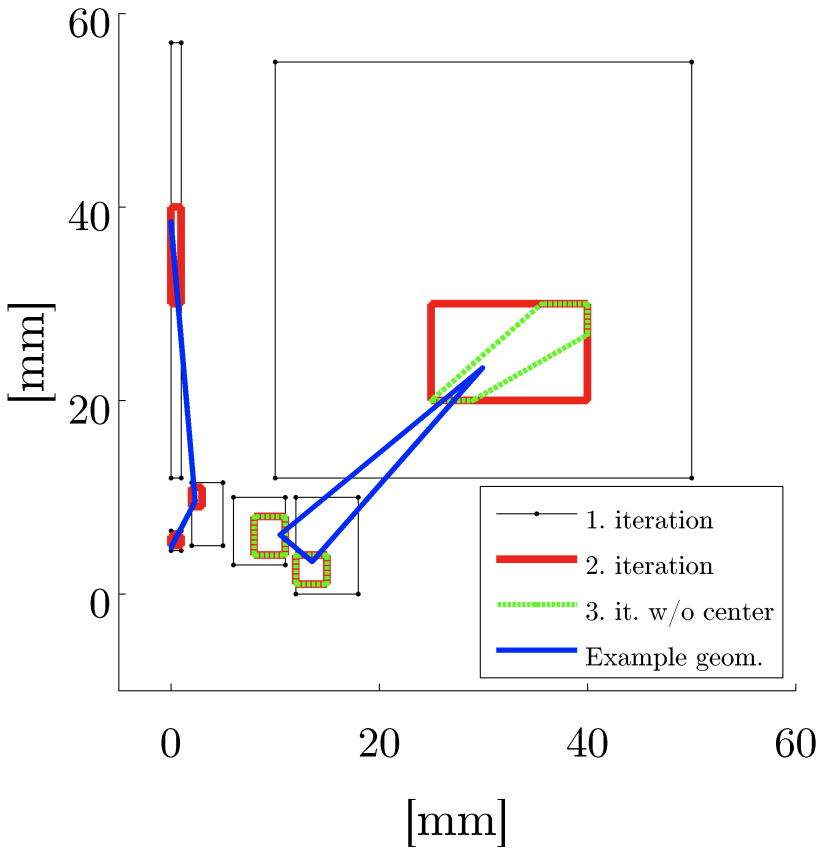

Figure 3.14: *Iterative narrowing of waveguide geometry search space.*

At the stage where a promising geometry of the type shown in 3.13I was chosen for prototype development, an analysis was performed of the geometry without the center reflector (like figure 3.13L). The performance difference was minimal under 16 kHz, and a last sweep was performed in the geometric search range shown in figure 3.14 (green). The choice to remove the centerpiece was not only based on performance, but also on the

possibility to achieve a reduction in production complexity and cost.

Several hundred geometries of the type shown in 3.13K were analyzed in an automated process, but the results were not promising, and the geometry type was subsequently discarded. In the end over 1200 different geometries were analyzed and the waveguide that best matched the design criteria was chosen for prototype development.

3.4.1 Objective evaluation of waveguide performance

For any automated optimization, an objective function describing the relative merit of the current geometry must be calculated. An objective function for this type of optimization will be computationally expensive, as a full FEA of the geometry is needed for each evaluation. The use of BEM might reduce the computational cost of the objective function.

Some loudspeaker optimization methods can be found in [47, 56, 90–98]. Morgans et al [90] presents a fast and reliable gradient free optimization technique (Efficient Global Optimization) for computationally expensive objective functions, and shows that it is capable of producing a horn shape that provides a constant beamwidth above a certain limiting frequency. However, the optimization is only a 2-parameter spline representation of a horn expansion with a single design objective (smooth, frequency independent beamwidth).

Morgans et al [90] present the following equations for a single objective evaluation function

$$\Phi_1 = mean(\beta(\mathbf{f} \geq f_{min})) \tag{3.1}$$

$$\Phi_2 = std(\beta(\mathbf{f} \geq f_{min})) \tag{3.2}$$

$$S = \frac{\Phi_2}{\Phi_1} \tag{3.3}$$

where $\beta(\mathbf{f})$ is the vector of beamwidths calculated over a range of frequencies represented by a vector $\mathbf{f}$, and S is an objective measure of the beamwidth smoothness. The operator $\mathbf{f} \geq f_{min}$ selects only those frequencies above a cutoff frequency f_{min}, as the loudspeaker has a more omnidirectional radiation pattern at LF. The beamwidth smoothness increases over the considered range of frequencies when S decreases. Therefore, the objective of the optimization can be defined as the minimizing of S.

The design criteria presented in this thesis are more extensive than previous studies of optimization, and an objective evaluation function is consequently harder to find.

A number of attempts to automate the performance evaluation of the simulated waveguides were made during the development of the design method in this project. A method of evaluating the performance objectively would be very beneficial, as it would

- allow for sorting of the different waveguide geometries by performance;
- allow for automatically reduction of the geometric search space;
- make the visual inspection of the waveguide simulations redundant;
- enable the use of mathematically defined optimization methods.

Especially design criterion 2 (see Section 1.2), which deals with the correction of the on-axis response by passive filters, can be hard to quantify. Design criteria 4-6 are also nontrivial to evaluate objectively.

At first glance, the relative response should not be too difficult to quantify, as the ideal response should be flat and smooth at all angles. However, a plotting of the geometries in a *Geometry goodness plot* as shown in figure 3.15 presents a mapping that only partially correlates well with visual inspection of the simulation results. The selected waveguide number for prototype development is highlighted in blue, and the geometries in grey are the rest of the geometries from the final search space iteration (see figure 3.14). The numbers highlighted in red are a first selection of promising geometries from the visual inspection.

The y-axis represents a measure of flatness given by

$$\sum_{\theta=0}^{52.5^\circ} (std^2(\Omega_\theta(\mathbf{f})) + mean^2(\Omega_\theta(\mathbf{f}))) \tag{3.4}$$

where $\Omega_\theta(\mathbf{f})$ is the relative frequency response at a certain angle θ and $\mathbf{f}$ is a vector of the essential frequency range from 1.7-15 kHz. The x-axis represents

$$\sum_{\theta=0}^{52.5^\circ} std(\Omega_\theta(\mathbf{f})). \tag{3.5}$$

Low values on the x- and y-axis are beneficial, as they represent relative frequency responses which are flat and smooth. The goal of the plot presented

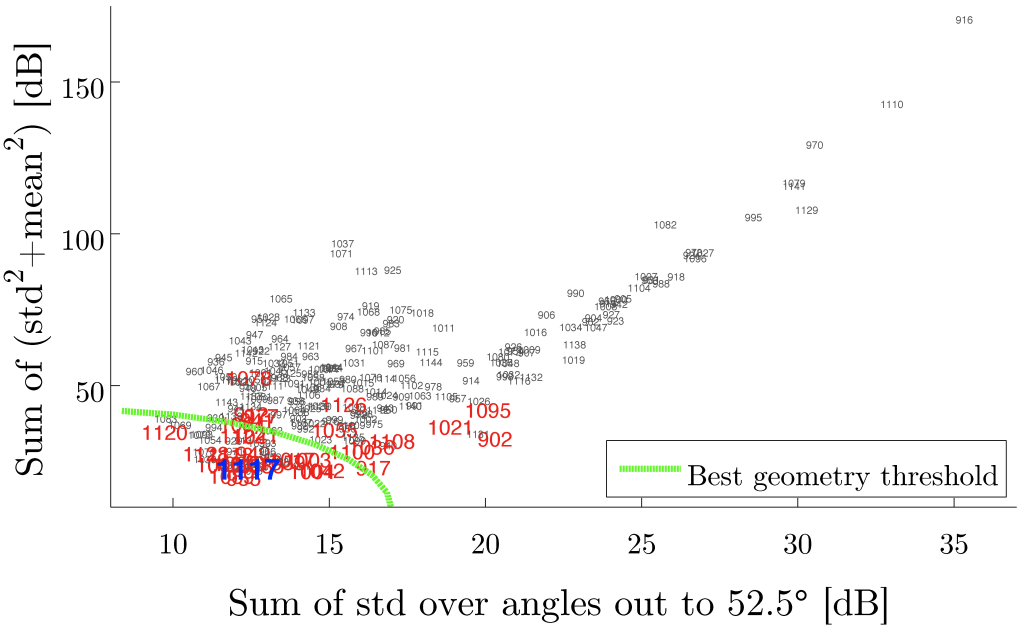

Figure 3.15: *Geometry goodness comparison mapping. Prototype waveguide numbers highlighted in blue, a first selection of promising geometries highlighted in red and the remaining geometries from final search space iteration in grey.*

in figure 3.15 is to assist the loudspeaker designer in the screening and decision making process. The geometry chosen for prototype development is not the best candidate solely based on the figure. However, the figure is only an attempt to sort the geometries based on the first design criterion. The other criteria must also be considered when deciding on the best overall performance.

3.4.2 Multi-objective optimization

If an objective evaluation of each design criterion could be made, a linear weighting function could be formed with a numerical description of the importance and priority of each criterion. This is called a single aggregate objective function (AOF), which is a combination of all the objective functions into a single functional form. As a consequence of this, the problem can be solved by a single-objective optimizer.

The design compromises can be expressed in an assembled weighting

function, and the function is used to globally evaluate the performance of the given waveguide geometry. The weighted sum approach minimizes the function F, given by

$$minF = w_1 f_1(\mathbf{x}) + w_2 f_2(\mathbf{x}) + ... + w_i f_i(\mathbf{x}) \tag{3.6}$$

where i is the number of design criteria represented by an objective evaluation function f_i, $\mathbf{x}$ is the vector of optimization or decision variables, and w_i are subjective weighting functions representing the trade-offs and prioritization. The obtained solution will depend on the the subjectively specified scalar weights for each objective. Additionally, each objective function could again have its own weighting functions. As an example, the importance of smoothness is greater at angles closer to the axis.

Complexity is added to an optimization problem when several objectives are present. Normally there is no single solution to such problems, no definitive optimum in the sense traditionally expected. Instead, a large family of alternative solutions exists where there are different balances of the various objectives. A trade-off between these objectives exists, and these compromises are known as a *Pareto set*. A change that makes at least one objective better without making any other objective worse is called a *Pareto improvement*. A solution is judged to be *Pareto optimal* if it is not dominated by other designs; it is better than another design in at least one aspect and that no further Pareto improvements can be made. In applied mathematics, multimodal optimization deals with tasks of finding all or most of the multiple solutions, as opposed to a single best solution.

The diversity of solutions precludes the notion of a 'right' or 'wrong', and decisions must be made based upon the full dynamic context of the situation. Optimization problems often possess several good solutions, and obtaining these solutions is the goal of a multi-modal optimizer. The solutions could all be globally good, or a mix of globally and locally good solutions. Evolutionary algorithms are often used for solving multi-objective optimization problems, and most apply Pareto-based ranking schemes. Some information on multimodal optimization can be found in [99–101].

Comsol has an optional optimization module, which has been used in a tutorial project to optimize horn loudspeakers [102]. Unfortunately, the license for this module was unavailable during the course of this project. The method of design automation applied in this project is not optimization in a strict mathematical sense as discussed previously.

3.5 Prototype construction

The dimensions of the selected final waveguide were sent to SEAS, who subsequently constructed a 3D CAD drawing of the waveguide. The prototype was 3D printed in plastic and measured by SEAS in the way described in Section 3.1. A picture of the finalized prototype is shown in figure 3.16. Measurements with damping applied to the outer edge of the cone (as seen in the figure) were also performed in order to study the effect of the mounting legs.

Figure 3.16: **Upper left:** *Prototype measurement setup (with damping)* **Upper right & bottom:** *Prototype waveguide mounted on tweeter.*

Chapter 4

Results

This chapter presents the results of the FEA and the prototype measurements.

4.1 Solving

Some computational information of a typical waveguide is shown in table 4.1. The MATLAB script can run about 160 geometries during the course of 8 hours on a normal desktop computer with an *Intel Core 2 Duo 2,4 GHz* CPU. Solution time is directly proportional to CPU speeds, so an upgrade to a state of the art multicore processor will lead to a substantial increase in computational efficiency. The size of the random access memory (RAM) used is not really an issue when dealing with 2D problems of this size.

DOF	22k
No. of elements	9k
Solution time	2-3 minutes
No. of frequencies	30 (1.25-20 kHz)
Mesh area	7300 mm^2

Table 4.1: *Computational information of typical waveguide*

4.2 Comparison of simulated and measured 27TFF tweeter

The following section presents results from anechoic measurements and COMSOL simulations of the 27TFF tweeter.

The simulated sensitivity of the tweeter at different angles is presented in figure 4.1, where 0° is on-axis. The corresponding measurements can be seen in figure 4.2. The resonance peaks and dips at 17-18 kHz in figures 4.1 and 4.2 are very similar. The deviation between the measured and simulated sensitivity of the baseline model can be seen in figure 4.3. The simulated tweeter is 2-5 dB more sensitive than the measurements for all angles in the frequency range from 2.5-10 kHz. The deviations on-axis are small at frequencies higher than 10 kHz, while being quite large at increasing angles. The sensitivity is underestimated in the simulation at most angles below 2 kHz.

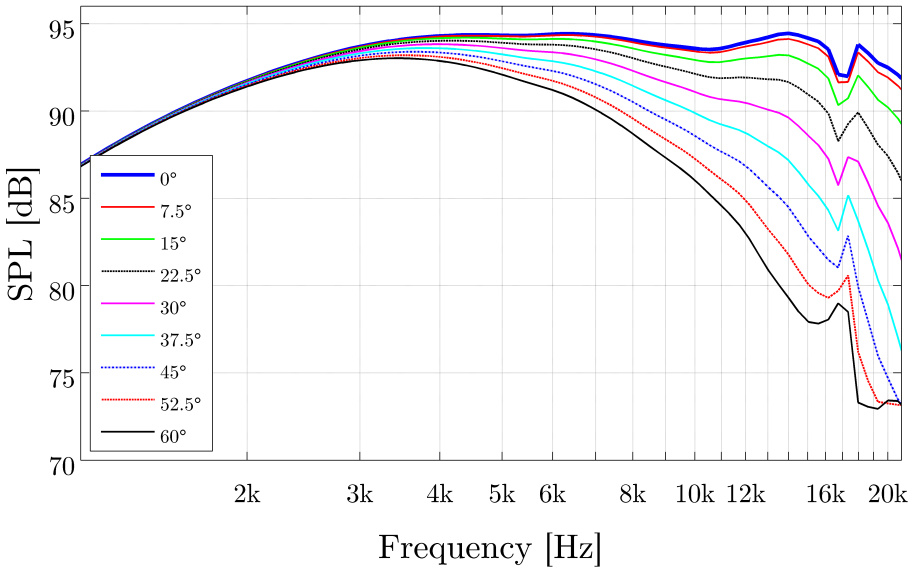

Figure 4.1: *Simulated sensitivity of the 27TFF tweeter model.*

The simulated frequency response at the same angles normalized to the on-axis response is shown in figure 4.4 in solid lines, while the measured response is shown in dotted lines. Figure 4.5 presents the deviation between simulated and measured sensitivity (normalized to their respective on-axis

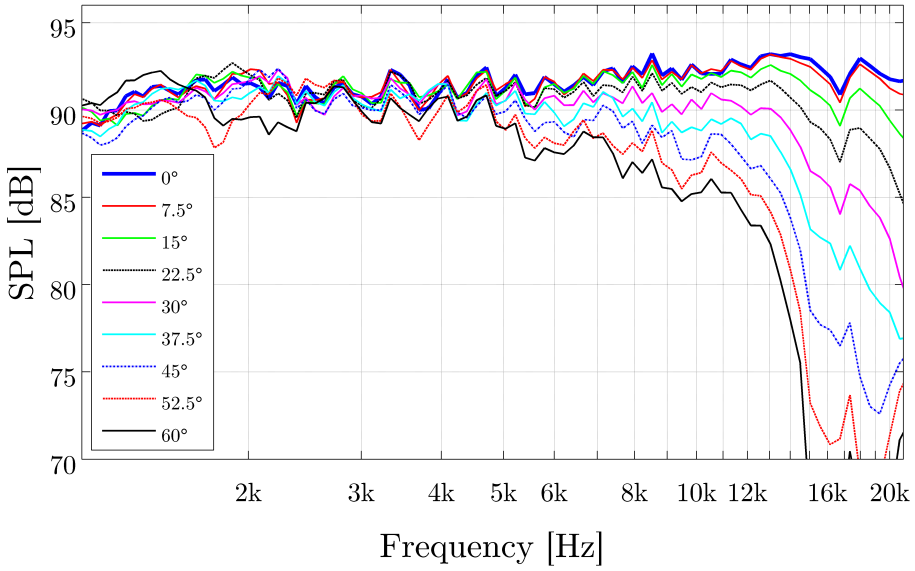

Figure 4.2: *Measured sensitivity of the 27TFF tweeter.*

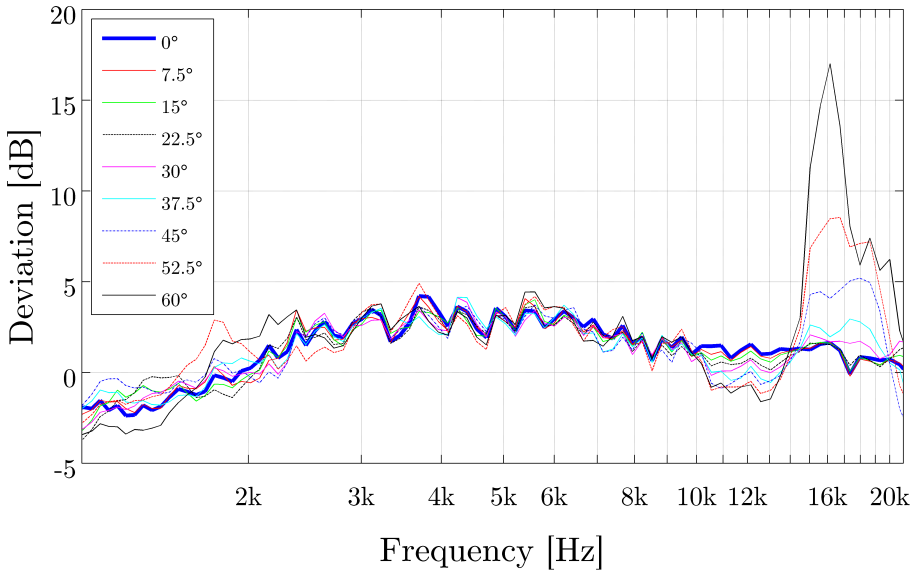

Figure 4.3: *The deviation between simulated and measured sensitivity for the 27TFF tweeter.*

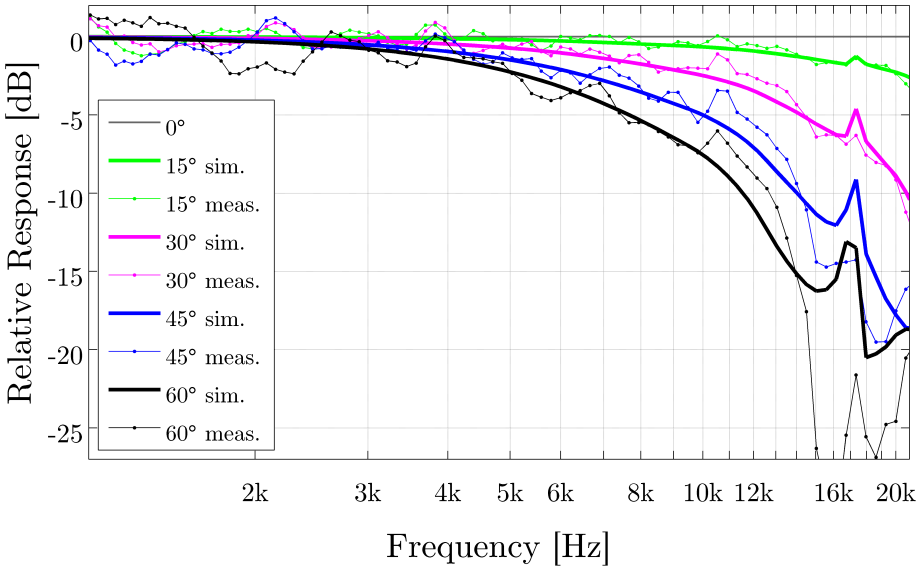

Figure 4.4: *Measured and simulated relative response (normalized to their respective on-axis responses) of the 27TFF tweeter.*

responses). As can be seen from the figure, the errors are relatively small (±2 dB) for all angles under 14 kHz. Above 14 kHz, the errors increase at 45° and 60° off-axis. The errors generally increase with increasing angles off-axis.

Figures 4.6 and 4.7 show the measured and simulated current and impedance, respectively. There is a clear mismatch in the resonance frequency, and there is generally poor accordance between the model and measurements of current. However, the impedance converges at frequencies above 5 kHz.

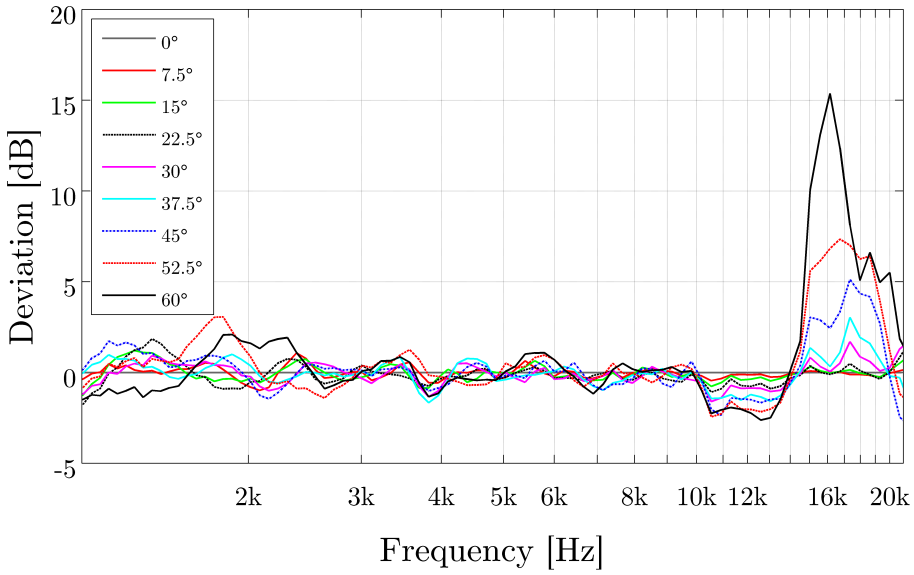

Figure 4.5: *The deviation between simulated and measured sensitivity (normalized to their respective on-axis responses) for the 27TFF tweeter.*

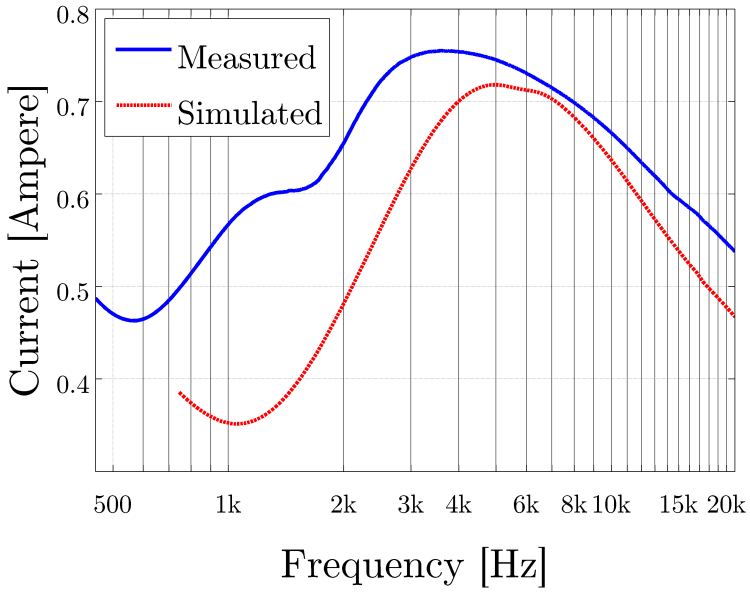

Figure 4.6: *Comparison of measured and simulated current in the voice coil.*

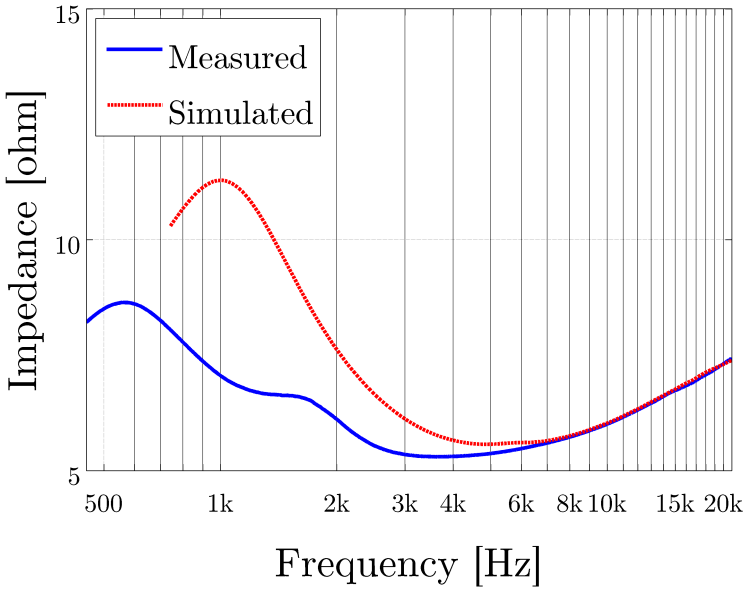

Figure 4.7: *Comparison of measured and simulated impedance (abs. value).*

4.3 Results from selected waveguide

The final waveguide geometry chosen for prototype development can be seen in figure 4.8. The simulated sensitivity and relative response is plotted in figures 4.9 and 4.10, respectively. The waveguide renders a frequency response that is quite flat and smooth from 3-8 kHz at all angles up to 60°, before it steadily falls off at about 9 dB per octave. The response keeps within a range of ±3 dB up to 18 kHz at angles up to 45°. At 60°, large dips in the response occur at 15 kHz and 19 kHz.

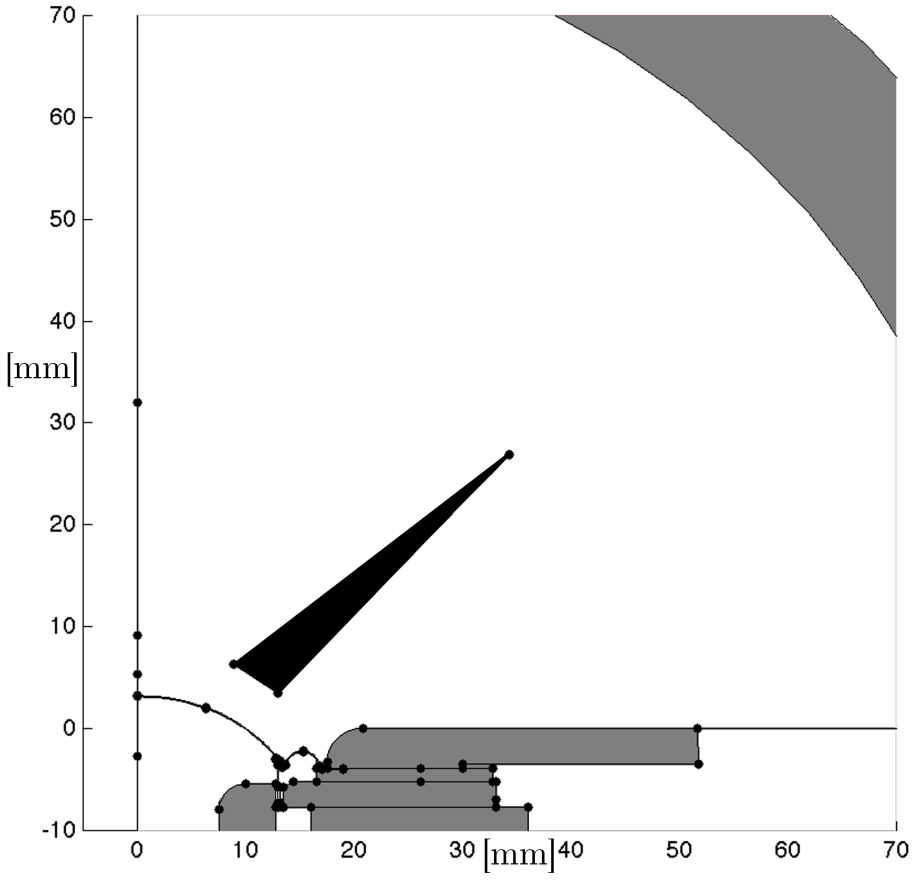

Figure 4.8: *Waveguide geometry #1117.*

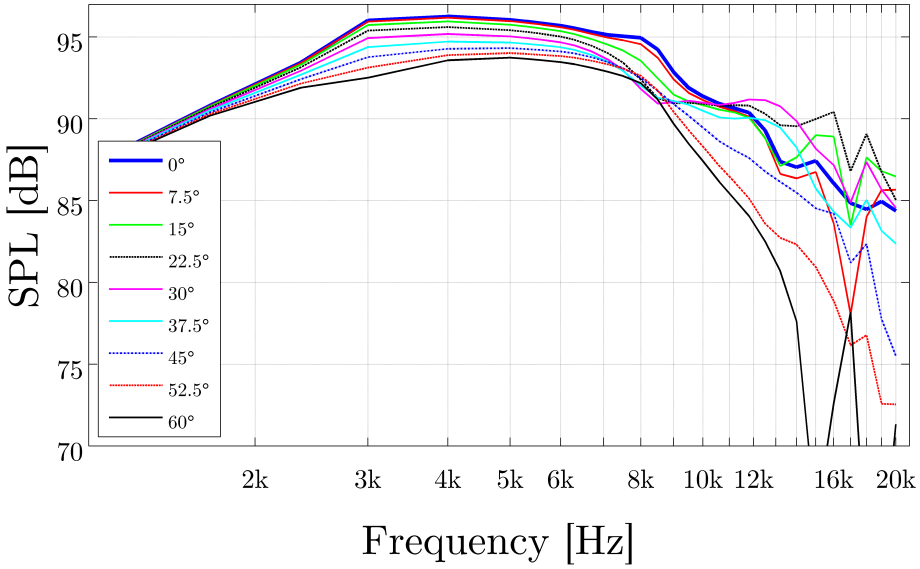

Figure 4.9: *Simulated sensitivity with waveguide geometry #1117.*

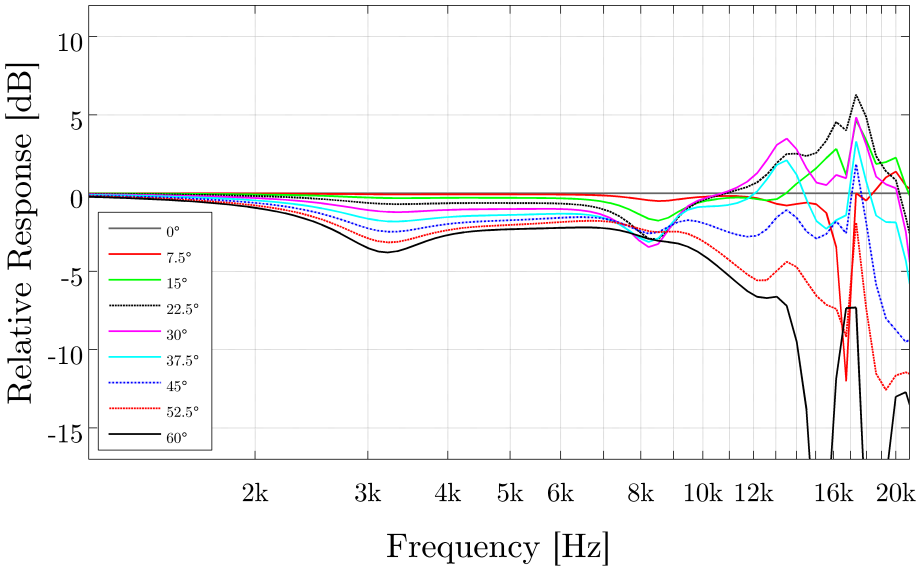

Figure 4.10: *Simulated relative response, waveguide geometry #1117.*

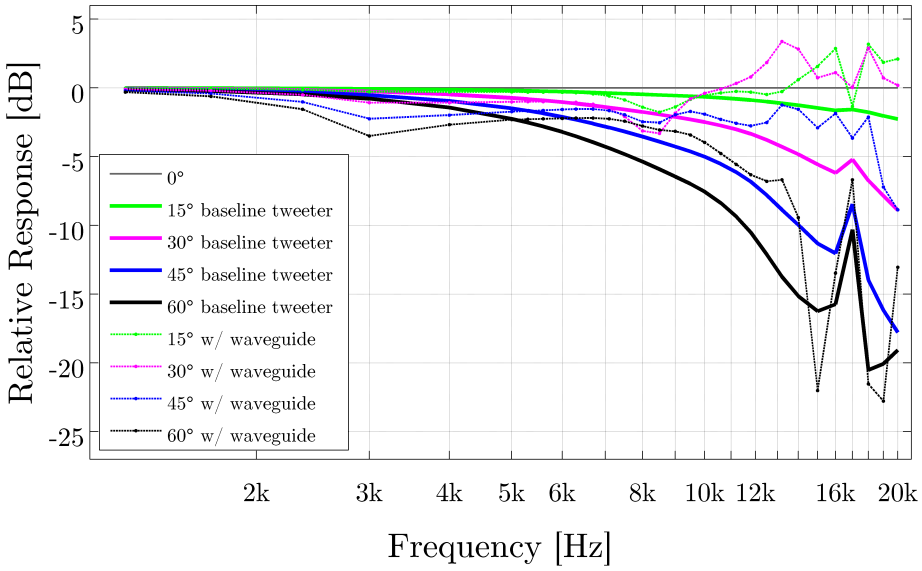

Figure 4.11: *Simulated relative response of tweeter with and without waveguide for geometry #1117.*

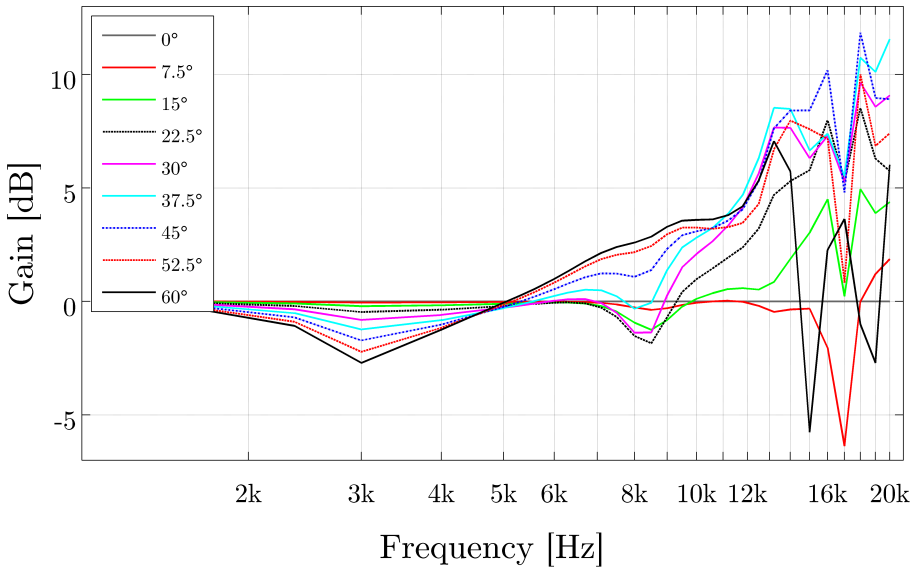

Figure 4.12: *Gain of waveguide compared to the baseline tweeter (relative response) for geometry #1117.*

Figure 4.11 plots the simulated relative response of the tweeter with and without the selected waveguide. Figure 4.12 clarifies the difference between the two, by plotting the gain of the waveguide compared to the baseline tweeter. The figures show that the waveguide tends to exchange a directivity decrease at LF (2-6 kHz) for a general increase at HF. The general HF gain of the waveguide at all angles is obvious, although there are some narrow dips with negative gain at 7.5° and 60° off-axis.

A simulation was performed on a version of the selected waveguide with rounded edges. Rounding the edges closest to the waveguide had no noticeable effect, but rounding the top edge had some minor impact on the responses above 16 kHz.

Wave propagation in the selected waveguide can be seen in 4.14 and a three-dimensional revolution of the 2D surface can be seen in figure 4.15.

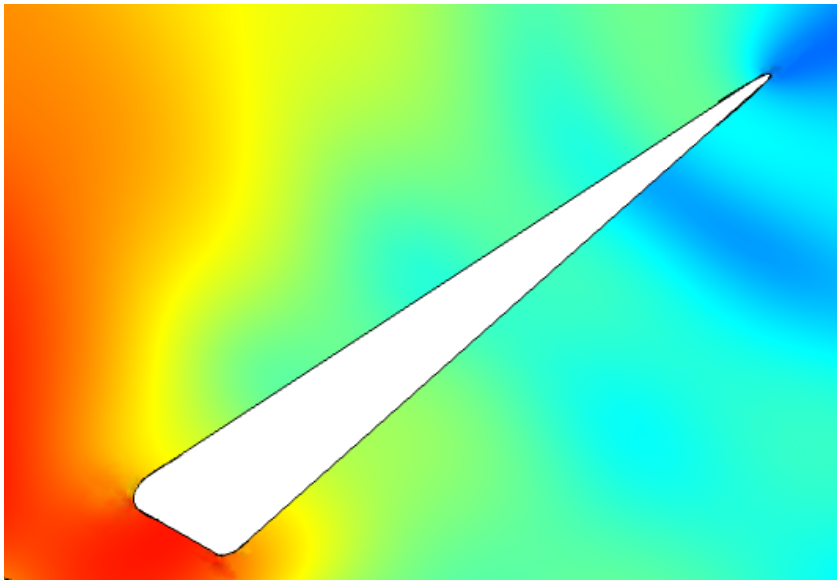

Figure 4.13: *Rounding of edges on waveguide geometry #1117.*

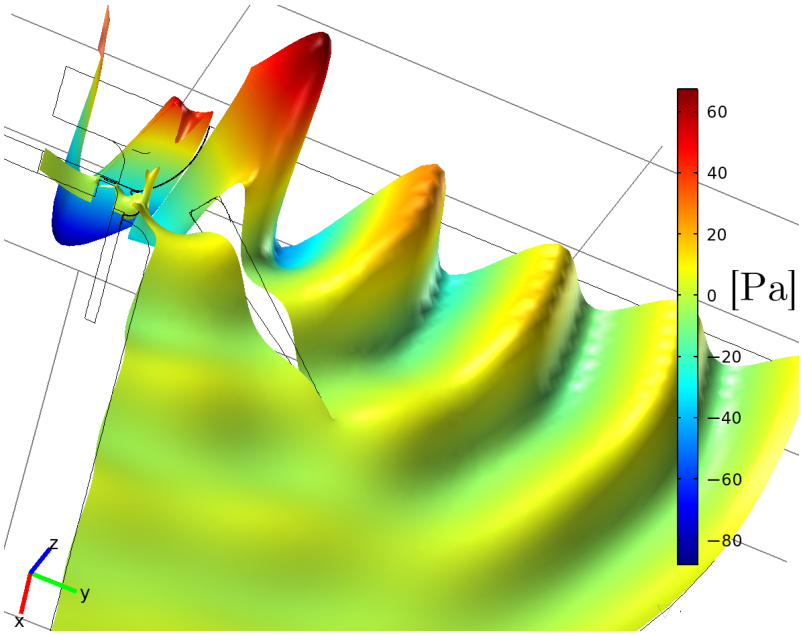

Figure 4.14: *Wave propagation in waveguide geometry #1117 @20 kHz.*

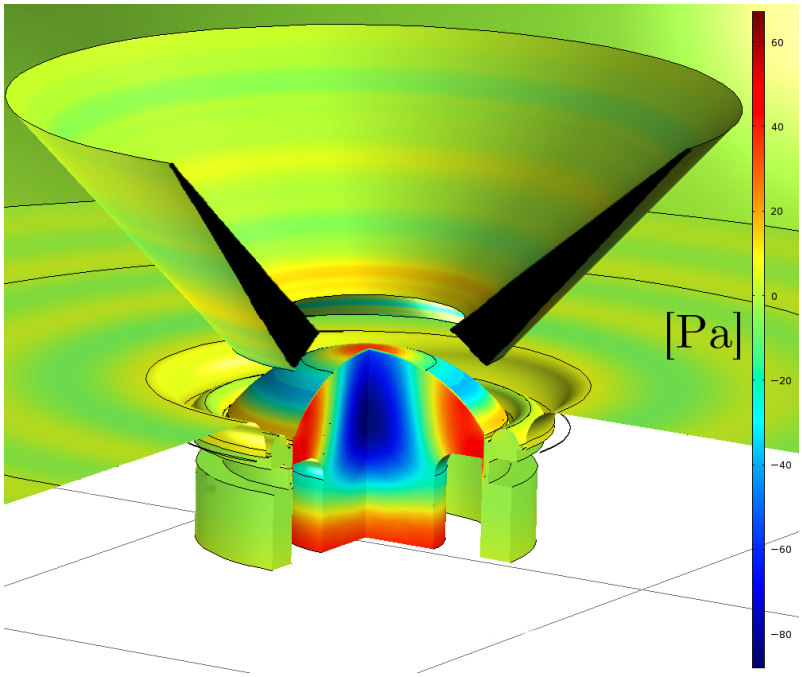

Figure 4.15: *Waveguide geometry #1117 @20 kHz in 3D (270° revolution).*

4.4 Waveguide prototype measurements

The measured sensitivity of the prototype at angles up to 60° off-axis is presented in figure 4.16. The on-axis response has a clearly visible 6 dB dip at 10-11 kHz, and also a very deep dip at 17 kHz.

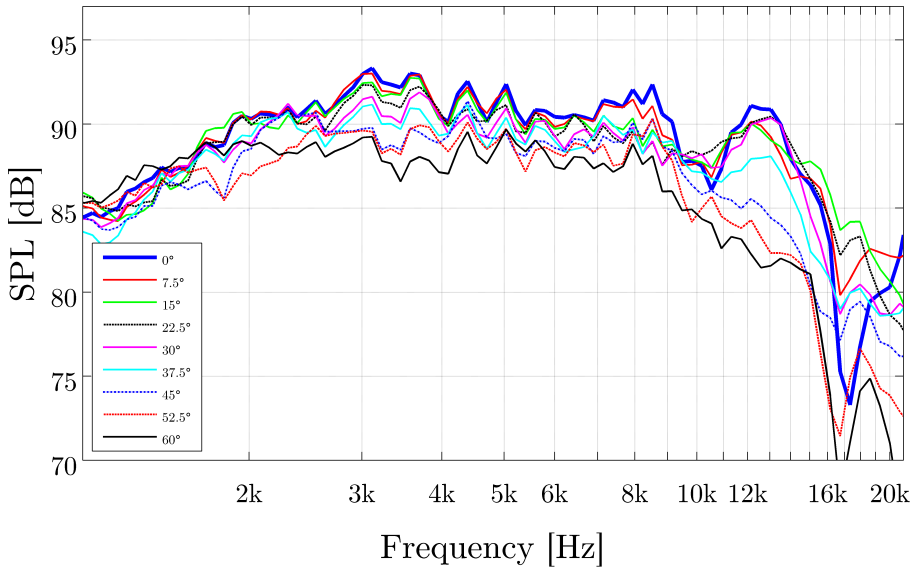

Figure 4.16: *Measured sensitivity of prototype.*

The deviation between the measured and simulated sensitivity of the prototype can be seen in figure 4.17. The simulations overestimated the sensitivity by 2-6 dB up to 11 kHz, but the spread and jaggedness for the various angles is quite small. At frequencies above 11 kHz, the deviations are substantial. The on-axis deviations are within 12 dB. Deviations at 60° are not unexpectedly even larger, as the baseline model displayed similar inaccuracies.

The frequency responses normalized to on-axis for all angles are shown in figure 4.18. As can be seen, the waveguide displays very well-behaved and smooth directional properties up to 11 kHz. Above this frequency, the relative response is more erratic, although there is still considerable HF disperion. A notable peak in the relative response appears at 17 kHz, as a consequence of the substantial dip in the on-axis frequency response seen in figure 4.16. Figure 4.19 shows the simulated and measured relative response

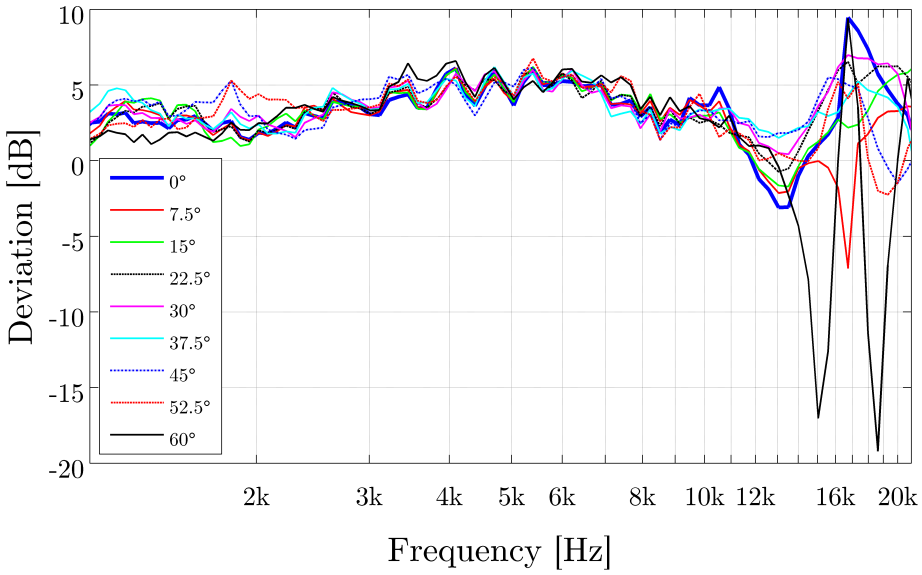

Figure 4.17: *Error of simulated sensitivity relative to prototype measurements.*

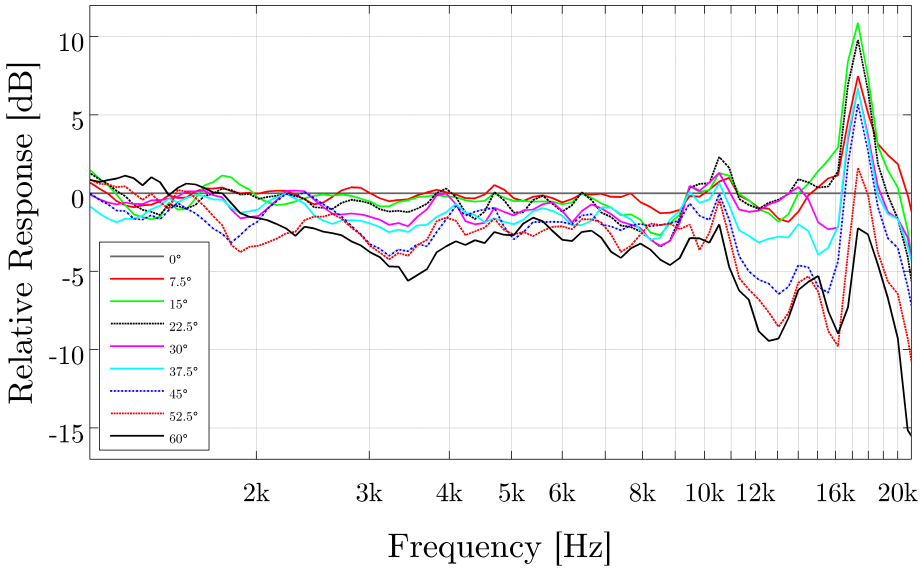

Figure 4.18: *Measured relative response of prototype.*

of the prototype plotted alongside each other for a selection of angles.

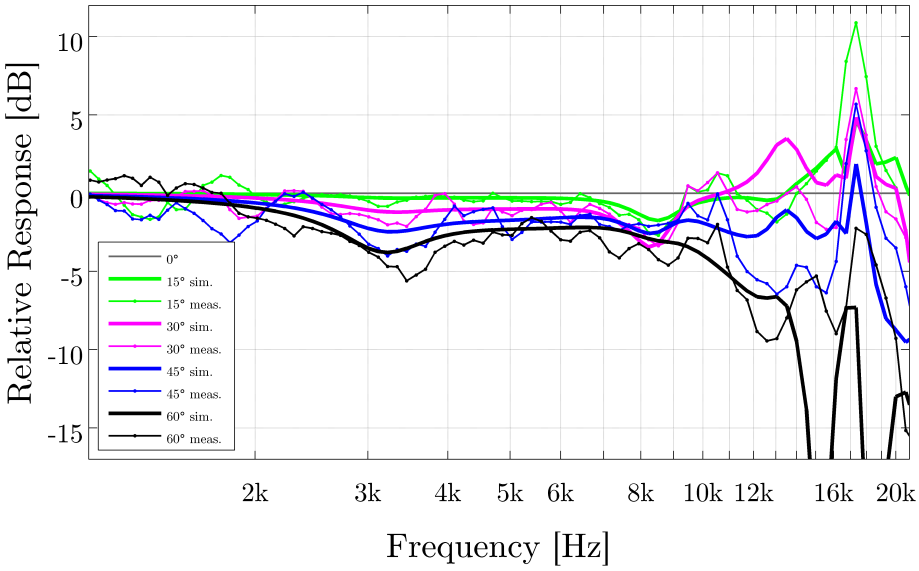

Figure 4.19: *Measured and simulated relative response of prototype.*

Figure 4.20 presents the deviation between simulated and measured directivity, by plotting the error between simulated and measured relative responses. As can be seen from the figure, the deviations are quite small (±2 dB) for all angles under 12 kHz. Above this frequency, the errors increase, especially at 7.5° & 60°.

Figure 4.21 shows the measured relative gain of the waveguide prototype compared to the baseline tweeter at all angles. The waveguide gives a substantial increase in HF dispersion above 9 kHz, with the exception of a dip between 11-13 kHz, where the waveguide is ineffective, but not detrimental.

The sensitivity of the prototype with damping applied along the outer edge of cone is presented in figure 4.22, and the effect is insignificant compared with the waveguide without damping (figure 4.16). The damping creates very small changes in the measured response, with the exception of a 3 dB decrease from 2.5-6 kHz and slightly decreased dispersion around 8 kHz.

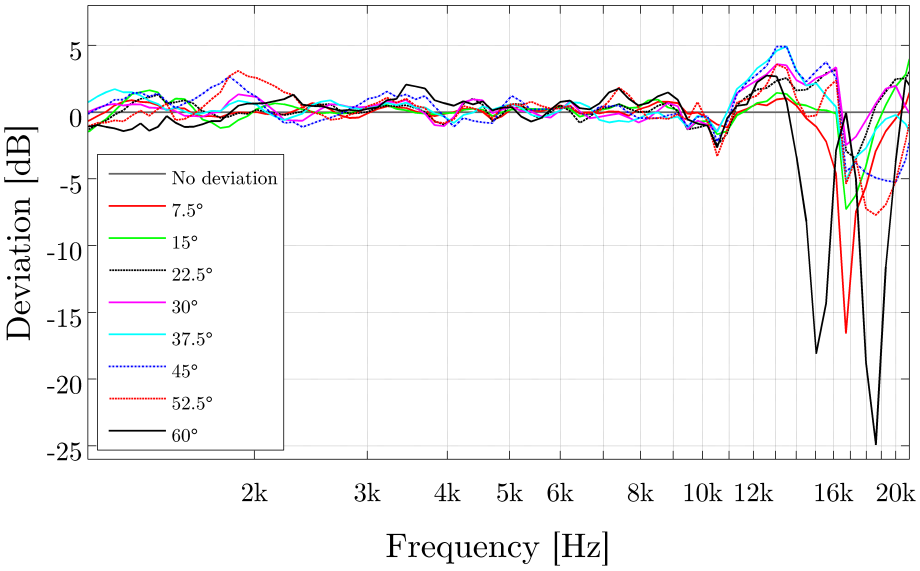

Figure 4.20: *Deviation of simulated directivity relative to prototype measurements.*

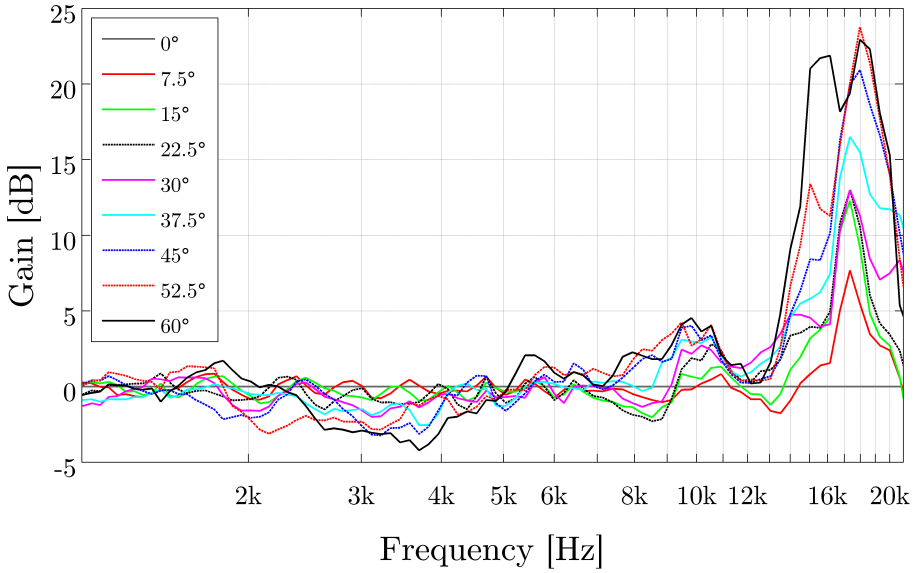

Figure 4.21: *Measured relative dispersion gain of prototype compared to baseline tweeter measurements.*

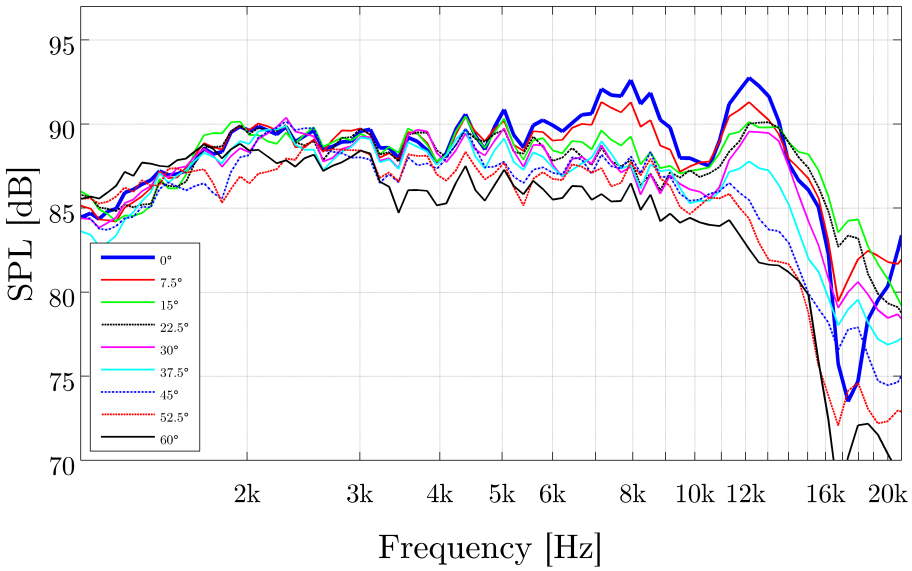

Figure 4.22: *Measured sensitivity of prototype with damping applied along the outer edge of cone.*

Chapter 5

Discussion

This chapter discusses the results of the FEA, the presented design method and the performance of the constructed prototype waveguide.

5.1 Baseline model accuracy

The deviation between the measured and simulated sensitivity of the baseline model as seen in figure 4.3 is tolerable and quite smooth over a large part of the relevant tweeter bandwidth. The jaggedness of the response could be due to some measurement errors. The resonance peaks and dips at 17-18 kHz in figures 4.1 and 4.2 are quite accurately modelled, although the source of the resonance is unknown. If the on-axis frequency response was the main design criterion, an accuracy of ≈5 dB in sensitivity would be unsatisfactory.

The measurements are not done in an infinite baffle, as the simulations are. This might be a reason for some of the discrepancies in the simulation-measurement comparisons.

As a flat and smooth relative frequency response is the main design criterion for this waveguide, the model accuracy of this parameter is more critical than the on-axis frequency response. Figures 4.4 and 4.5 show an excellent coherence between model and measurement over most of the relevant tweeter operating range.

Over 14 kHz, in the upper part of the hearing range, the directivity modelling errors are large at angles over 30°. The reasons for these errors are not apparent, but the most likely explanation is that the diaphragm movement and breakup modelling is inaccurate.

A distinct dip is noted at 16.8 kHz, which is equivalent to a wavelength of 20 mm. Anthony [61] found a similar dips in his FEA model of a tweeter,

and related them to the diameter of the dome and dome height (quarter wavelength). Although the dome moves quite pistonic, the phase shift due to a 7 mm dome height is considerable. However, it is uncertain if these explanations are applicable to the tweeter model in this project.

Henwood and Geaves [58] used an acoustic center placed at one cone radius in front of the plane of the cone outer edge in order to make the LF responses converge. At LF the flow pattern of the air in front of the driver seems to emanate from this point. The acoustic center is the center of curvature of the acoustic waves, and not necessarily the physical source [103, 104]. However, the apparent acoustic center is dependent on frequency, and the behavior is not always predictable. It would be impractical to move the measurement points based on the apparent acoustic center for each frequency studied.

The model implemented in this project has the acoustic center placed a little inside the tweeter dome, in line with the baffle. This may be a reason for the deviations at LF.

The mismatches between measured and simulated voice coil current and impedance are likely due to inaccurate material properties in the model. The differences are largest at lower frequencies, and the model accuracy is not critical in this bandwidth. Few previous studies developed an acoustic-structure interaction model of a tweeter, and there are reasons to believe that errors for small geometries are larger than for woofers. Macey [105] suggests that the effect of inaccuracies in material parameters of glue such as Young's modulus could be more drastic on smaller drivers.

The model will likely be more inaccurate at extreme resonance points than in reality, as the accuracy of the damping properties at these frequencies will be of great importance.

The model indicates a resonance frequency of around 1 kHz instead of the measured driver's 550 Hz, which indicates that the mass is too high or that the stiffness is to low. Salvatti [47] and Murphy and Morgans [50] has had some experience with errors in resonance frequency due to errors in mass, stiffness, or applied damping as well. Salvatti discovered that the material thickness of the simulated surround was different from the physical driver, leading to a higher stiffness. Anthony [61] states that errors around the fundamental mass-stiffness resonance of the moving system and the first breakup mode of the dome are largely due to the use of frequency-independent material properties and that improvements can be achieved by allowing these properties to vary with frequency. However, very good agreement can be gained in the passband.

The model accuracy could be improved by manually tuning the model parameters and material properties to match up with measurements. Laser velocimetric measurements can be performed on the tweeter in order to gain further insight in the model anomalies. This type of measurement can also verify if the simulation of the diaphragm breakup is correct. However, a decision was made to proceed with the waveguide design, as the directive properties of the model sufficiently matched the measurements in the frequency range of interest.

Viscous effects may potentially be significant in narrow gaps (such as the magnet gap) [105]. Comsol solves the linear wave equation, so the effects of viscous damping in small cavities or non-linear behavior of air at high SPLs are not modelled [50].

Laminar flow resistance can become of importance and acoustic losses occur. Computational fluid dynamics may be necessary for a rigorous analysis of these phenomena. The pressure acoustics application mode in Comsol does not model this, and Hedges [52] solved the problem by creating new subdomains of air in the relevant gaps and applying a damping factor in terms of the bulk viscosity. Macey [105] also adopted a simplified approach in the geometry of air in a gap of constant thickness between two parallel infinite rigid isothermal planes. The linearized Navier Stokes, continuity, energy and ideal gas equations can be solved to first order, predicting a complex speed of sound for acoustic propagation in this gap. This approximation is not valid if the airflow through the gap is turbulent, and it does not consider the temperature dependent property of viscosity.

No such implementation as suggested by Hedges or Macey was made in the simulations in this thesis. The potential problems with laminar flow resistance is one of the motivations of design criterion 6 from Section 1.2, which urges the designer not to develop waveguide geometries with narrow gaps.

In version 4.2 of Comsol, thermal acoustics is implemented as a dedicated module, and accurate solutions for small cavities with thermal conduction and viscous losses coupled to the sound field can be obtained in a straightforward, but very computationally expensive way [106]. Large modelling errors at LF are expected in narrow gaps smaller than 1 mm if thermal acoustics is not accounted for, and the magnet gap is well below this limit. Acoustic boundary layers are introduced, where thermal gradients and velocity gradients are important. At HF the boundary layer is much smaller and becomes less significant.

The modelling assumption of axial symmetry is generally a good one. However, in an axisymmetric model, the response to azimuthal forces is not included [35]. Asymmetric modes are usually considered acoustically negligible as the sound pressures radiated from parts of the diaphragm vibrating out of phase tend to cancel each other in the far field. However, such modes create off-axis responses that would depend on the azimuth angle [58]. Salvatti [47] performed numerous laser vibrometric measurements of real transducers, where decomposition of the SPL into radial and circumferential components shows that the non-axisymmetric contribution (bell modes) is negligible and can usually be ignored. Jones [53] also found that whilst a certain amount of asymmetry is present in the real drive unit, it is not of great significance.

The force factor Bl (eq. 2.6) is assumed to be independent of voice coil position. Henwood and Geaves [58] found that some modes displayed significant variation with Bl. Modes that displayed significant axial motion were the ones most affected by high Bl values. Although the model was of a woofer with a different suspension setup and geometry, it is plausible that errors in Bl can alter some modes in the tweeter model as well.

Holm [82] has studied a range of methods for visualizing directivity. Several methods of presenting the directional data have been explored (2D and 3D directivity plots), and the plots that have been used throughout this thesis conveyed the most information in a compact and readable way.

An ideal software package for loudspeaker design would provide full coupling between magnetic, structural, viscous, acoustic, and thermal FEM models together with electrical circuits in a user friendly environment. However, the full coupling would result in very long solution times and in many cases the vast amount of information rendered would be unnecessary.

5.2 Optimization strategy

The ad hoc manner of the preliminary waveguide study is an obstacle when attempting to achieve the goal of total design automation. Unfortunately, it seems to be necessary to have a general geometric starting point in order to reduce the search space and avoid invalid geometries. As the response variations are quite large with small changes in geometry, one cannot dismiss the fact that possibly better (or equally good) types of geometries have been discarded in the preliminary waveguide study. Large variances

in performance with apparently small changes in geometry will also be important to assess, as this is essential when predicting possible production error variance.

A weakness of the method used to find the optimal geometry is the dependency of visual inspection. This can be time consuming and tiring when large datasets need to be reviewed. The construction of a method that effectively recognizes the best geometry is not a trivial task, as discused in Sections 3.4.2 and 3.4.1. Usually compromises between the different design parameters have to be made. As an example, a geometry with a perfect relative response would be less useful if the frequency response was impossible to correct with a passive filter. Such compromises could possibly be implemented in a weighting function, but an accurate weighting of design criteria is suspected to be hard to find.

The visual inspection was somewhat simplified by a rough sorting algorithm that discarded the geometries with very large standard deviations in their relative responses.

Toole [9] describes the process of visual inspection as relatively straightforward, involving looking for a flat, wide bandwidth on-axis response, and for consistently repeated patterns in the family of increasing off-axis measurements. He further states that the importance of the deviations from the underlying smooth contours must be weighted according to a set of rules that take account of the direction, shape, and magnitude of the irregularities, and the frequencies at which they occur. Visual "integration" of plots by experienced eyes can sort out much of the inconsistent clutter caused by interference effects, while revealing important persistent discontinuities and directional trends. The result of this type of inspection is a method for evaluating and ranking loudspeaker performance with about the same resolution and order as carefully and thoroughly performed listening tests, although in a considerably less time demanding and expensive way. A final selection can be made by careful trading off performance in one aspect against another.

The method proposed is by no means a perfect design algorithm, but there is unquestionable potential in this way of designing loudspeakers.

5.3 Selection of final waveguide design

The selected geometry for prototyping was chosen because of its very nice simulated directional properties up to 45° off-axis. The spread between all angles in the relative frequency response is very small up to 10 kHz. As such, the waveguide fulfills the primary design criterion, even though the relative response at 60° shows large variations at frequencies above 13 kHz (where the model is known to be somewhat inaccurate anyway, as discussed in Section 5.1). The simulations are promising and the waveguide is believed to give a considerable gain in listener experience compared to a typical direct radiator.

The frequency response is quite flat before it falls off steadily at HF from 8 kHz. It is believed that this type of on-axis response can be corrected adequately in a passive crossover/filter network, and hence meet design criteria 2 and 3. The waveguide creates a 1-3 dB increase in sensitivity from 2.5-8 kHz, and generally seems to exchange wider dispersion at HF for narrower dispersion at LF. The increased directivity of the waveguide at LF will be audible, although the change is much smoother (over a wide bandwidth) than the baseline tweeter. The increased directivity of a tweeter at the lower frequencies of its operating range is beneficial when matching the directivity of a mid-band driver at the crossover frequency.

The size of the waveguide is not particularly unpractical, and avoids very narrow gaps and extreme proximity to the diaphragm. Therefore, it complies to design criteria 4 and 6.

A thorough investigation of the effects of small geometric variations is beyond the scope of this thesis, but will be important related to the actual production of the waveguide. Consequently, it is difficult to state with certainty whether possible production problems will be avoided with this waveguide design.

5.4 Prototype performance

The directional properties of the prototype show excellent coherence with simulations up to 12 kHz, as seen in figure 4.20. The waveguide seems to utilize the on-axis dip at HF in order to match the decreased HF response off-axis, similar to the way described in the DXT patent [30]. The waveguide considerably increases the relative HF dispersion compared with the baseline tweeter, as was seen in figure 4.21.

However, there are some discrepancies between simulations and measurements that must be noted. The baseline model showed that errors in the modelling of directionality increased with angle and frequency (above 14 kHz). The same type of errors is found in the prototype measurements, although the errors are not predictable or evenly increasing with increasing angles. In addition to the sources of error discussed in Section 5.1, turbulence and other unpredictable behavior in the area between diaphragm and waveguide might be a source of simulation errors.

The prototype on-axis response is hard to correct with a simple passive filter, especially the dip at 9-11 kHz, although a digital filter is expected to be able to equalize it adequately. Even though our perception is less sensitive to narrow dips than peaks or broad band shelving, it is suspected that a dip like this will be clearly audible and detrimental.

As the conical horn shape is open at the sides, there will be path length differences around the waveguide. It is suspected that a construction like this will introduce interference effects that are highly spatially variable; the response will therefore be very dependent on measurement position. A higher spatial sampling in simulations and measurements could have illuminated these problems.

The damping applied to the outer edges did not affect the measured responses significantly, and it is therefore assumed that the influence of mounting brackets is negligible. Inaccurate physical representation of the prototype can be the source of the errors in measurement versus simulation, although it is unlikely as the 3D printing process is very accurate.

As mentioned in Section 1.1.2, floor and ceiling reflections are often unwanted. A waveguide does not necessarily benefit from having a wide directivity pattern in the vertical direction. An axisymmetric design and modelling method cannot be used to control the dispersion differently in the vertical and horizontal direction. The design algorithm presented in this thesis is entirely transferable to 3D, although the effectiveness will decrease as the computational demands and number of geometric variables increase.

5.5 Future work

There is much work to be done before a completely automated design algorithm can be operational. One of the main challenges is obtaining an accurate multi-objective evaluation function and implementing mathematical optimizers for this type of problem. A further understanding of the relation between directional properties and waveguide/reflector geometries would be a welcome advancement, as a more clever way of narrowing the geometric search space iteratively might be achieved. A completely automated design algorithm would be an effective way of prototyping loudspeakers.

Expanding the 2D problem to 3D is feasible, although with increased computational cost. A 3D approach would allow for asymmetric designs and thereby possibilities to reduce dispersion in the vertical direction, with the subjectively favorable effect of reduced floor and ceiling reflections.

The accuracy of the simulated baseline tweeter model can be improved, especially the directional properties at large angles off-axis. This will hopefully also increase the predictability of waveguide performance at HF. Including more advanced coupling of physical properties such as electromagnetic, thermal and viscous effects will be a natural way forward. However, obtaining accurate material parameters will be the most important step towards an accurate model at HF.

Chapter 6

Conclusion

In this work, a method of designing a wide dispersion waveguide using finite element analysis has been presented. A smoother and flatter transition of the frequency response at off-axis angles was defined as the primary design goal, related to research on subjective loudspeaker preferences.

Firstly, a baseline FE model of the SEAS 27TFFC soft dome tweeter was built in COMSOL MULTIPHYSICS. An acoustic-structure interaction was defined, and solved after using material properties and the measured blocked coil impedance as input. Subsequently, the model was verified by measurements.

The precision of material parameters are of utmost importance when building and creating a realistic representation of the loudspeaker behavior, and the deviations in frequency response and resonance frequency are mainly due to inaccurate material parameters. However, sufficient accuracy of the directional properties of the baseline model in the frequency range of interest enabled simulations of waveguides to be performed with reasonable confidence in their truthfulness.

Secondly, many waveguide geometry types were investigated, and a method of randomizing geometries and automating the simulation process was developed using the *Livelink for Matlab* module in COMSOL. The evaluation of each waveguide design was performed mainly by visual inspection, although efforts were made to objectively quantify this stage in the design process. Subsequently, a promising waveguide design was selected based on a compromise between the set of defined design criteria.

Thirdly, a prototype of the selected waveguide was built and the measured performance was compared to the simulated model. The

waveguide performed adequately, although deviations from simulations were larger than expected at HF. The measurements validate the modelling procedure and emphasize the value of the method as a design tool, even though the prediction accuracy can be improved. It can be inferred that a waveguide of this type can be an effective way to increase HF dispersion for a large range of commercially available tweeters with only small modifications.

The method of waveguide design presented in this thesis has, as far as the author is aware of, not been previously described in literature. Although some work has been done on modelling the acoustic-structure interaction of a tweeter, the coupling of this model to parameterized and randomized waveguide geometries is novel. The unique waveguide prototype can be used to increase the HF dispersion of a tweeter in a way that is not readily available today.

The thesis combines FE modelling, understanding of directivity and waveguides in order to virtually prototype loudspeakers. By utilizing computer simulations, the prototyping process can be more effective and the cost of building many prototypes reduced, all the while designing better performing loudspeakers.

References

[1] D. Moulton, "360 degree dispersion frequency invariant acoustic transduction system," in *81st AES Convention, Los Angeles, Convention Paper 2392*, 1986.

[2] L. L. Beranek, *Acoustics*. New York: McGraw-Hill Book Company, 1954.

[3] D. Moulton, "The Use of an Acoustic Lens to Control the High Frequency Dispersion of Conventional Soft Dome Radiators," in *American Loudspeaker Manufacturers Association Symposium*, 1998.

[4] SEAS, "DXT Concept Brochure." `http://www.seas.no/images/stories/prestige/pdfdatasheet/dxt_seas.pdf`, 1. June 2011.

[5] P. M. Morse and K. U. Ingard, *Theoretical Acoustics*. New York: McGraw-Hill Book Company, 1968.

[6] Siegfried Linkwitz, "Linkwitz Lab Website." `http://www.linkwitzlab.com`, 1. June 2011.

[7] F. E. Toole, "Subjective Measurements of Loudspeaker Sound Quality and Listener Performance," *J. Audio Eng. Soc.*, vol. 33, no. 1/2, 1985.

[8] F. E. Toole, "Loudspeaker Measurements and Their RelatiOnship to Listener Preferences: Part 1," *J. Audio Eng. Soc.*, vol. 34, no. 4, pp. 227–235, 1986.

[9] F. E. Toole, "Loudspeaker Measurements and Their Relationship to Listener Preferences: Part 2," *J. Audio Eng. Soc.*, vol. 34, no. 5, pp. 323–348, 1986.

[10] F. E. Toole, "The Acoustics and Psychoacoustics of Loudspeakers and Rooms-The Stereo Past and the Multichannel Future," *109th AES Convention, Los Angeles, Convention Paper 5201*, 2000.

[11] F. E. Toole, *Sound Reproduction: The Acoustics and Psychoacoustics of Loudspeakers and Rooms*. Focal Press, 1st ed., 2008.

[12] F. E. Toole, "Loudspeakers and Rooms for Sound Reproduction-A Scientific Review," *J. Audio Eng. Soc*, vol. 54, no. 6, pp. 451–476, 2006.

[13] S. E. Olive, "Differences in Performance and Preference of Trained versus Untrained Listeners in Loudspeaker Tests: A Case Study," *J. Audio Eng. Soc.*, vol. 51, no. 9, 2003.

[14] S. E. Olive, "A Multiple Regression Model for Predicting Loudspeaker Preference Using Objective Measurements: Part I - Listening Test Results," in *116th AES Convention, Berlin, Convention Paper 6113*, 2004.

[15] S. E. Olive, "A Multiple Regression Model for Predicting Loudspeaker Preference Using Objective Measurements: Part II - Development of the Model," in *117th AES Convention, San Francisco, Convention Paper 6190*, 2004.

[16] D. Queen, "Relative Importance of the Direct and Reverberant Fields to Spectrum Perception," *Audio Eng. Soc. (Project Notes/Engineering Briefs)*, vol. 21, pp. 119–121, 1973.

[17] D. Queen, "The Effect of Loudspeaker Radiation Patterns on Stereo Imaging and Clarity," *J. Audio Eng. Soc.*, vol. 27, pp. 368–379, 1979.

[18] D. Moulton, "The localization of phantom images in an omnidirectional stereophonic loudspeaker system," in *81st AES Convention, Los Angeles, Convention Paper 2171*, 1986.

[19] S. Linkwitz, "Hearing Spatial Detail in Stereo Recordings," in *26th Tonmeistertagung-VDT International Convention*, 2010.

[20] S. Linkwitz, "Investigation of Sound Quality Differences between Monopolar and Dipolar Woofers in Small Rooms," *105th AES Convention, San Francisco, Convention Paper 4786*, 1998.

[21] J. A. Pedersen and G. Munch, "Driver Directivity Control by Sound Redistribution," in *113th AES Convention, Los Angeles, Convention Paper 5648*, 2002.

[22] Limegreen, "Home Cinema." `http://www.limegreen.tv/pages/home-cinema`, 1. June 2011.

[23] M. F. E. Barron, "Measured early lateral energy fractions in concert halls and opera houses," *J. Sound & Vibration*, vol. 232, pp. 79–100, 2000.

[24] W. M. Hartmann, "Localization of sound in rooms," *Journal of the Acoustical Society of America*, vol. 74, no. 11, pp. 1380–1391, 1983.

[25] S. Bech, "Perception of timbre of reproduced sound in small rooms: The influence of the room and the loudspeaker position," *J. Audio Eng. Soc.*, vol. 42, pp. 999–1007, 1994.

[26] S. Bech, "Timbral aspects of reproduced sound in small rooms I," *Journal of the Acoustical Society of America*, vol. 97, pp. 1717–26, Mar. 1995.

[27] S. Bech, "Timbral aspects of reproduced sound in small rooms II," *Journal of the Acoustical Society of America*, vol. 99, no. 6, pp. 3539–49, 1996.

[28] S. Bech, "Spatial aspects of reproduced sound in small rooms," *Journal of the Acoustical Society of America*, vol. 103, pp. 434–45, Jan. 1998.

[29] R. Walker, "A Controlled-reflection Listening Room for Multi-Channel Sound," in *104th AES Convention, Amsterdam Convention Paper 4645*, 1998.

[30] M. G. Kragelund, "Waveguide Unit," *US patent 20090154750*, p. issued 18. June, 2009.

[31] Peter Aczel, The Audio Critic, "Bang & Olufsen BeoLab5." `http://theaudiocritic.com/plog/index.php?p=ViewArticle&articleId=34&blogId=1`, 1. June 2011.

[32] Nacsound Loudspeakers, "Website." `http://www.nacsound.it/eng/indexeng.html`, 15. June 2011.

[33] Duevel Loudspeakers, "Website." `http://www.duevel.com/home/loudspeaker.shtml`, 15. June 2011.

[34] Mirage Loudspeakers, "Website." `http://www.miragespeakers.com/na-en/products/home-theater-system`, 15. June 2011.

[35] D. Henwood and G. Geaves, "Finite Element Modelling of a Loudspeaker Part 1: Theory and Validation," in *119th AES Convention, New York, Convention Paper 6582*, 2005.

[36] F. J. M. Frankort, "Vibration Patterns and Radiation Behavior of Loudspeaker Cones," *J. Audio Eng. Soc*, vol. 26, no. 9, pp. 609–622, 1978.

[37] A. J. M. Kaizer and A. Leeuwestein, "Calculation of the Sound Radiation of a Nonrigid Loudspeaker Diaphragm Using the Finite-Element Method," *J. Audio Eng. Soc*, vol. 36, no. 7/8, pp. 539–551, 1988.

[38] A. Dobrucki, P. Pruchnicki, and B. Zoltógórski, "Computer Modeling of a Loudspeaker Vibrating System," in *100th AES Convention, Copenhagen, Convention Paper 4207*, 1996.

[39] G. Pellerin, J. Polack, and J. Morkerken, "Finite Element Methods and Equivalent Electrical Models for Loudspeaker Characterization.," in *114th AES Convention, Amsterdam, Convention Paper 5743*, 2003.

[40] D. Henwood, J. Moore, G. Geaves, and P. A. Fryer, "Towards the Transient Modelling of Loudspeaker Diaphragm/Surround Boundaries," in *108th AES Convention, Paris, Convention Paper 5166*, 2000.

[41] P. A. Fryer, D. Henwood, M. Jon, and G. Gary, "Verification of an approach for transient strucural simulation of loudspeakers incorporating damping," in *110th AES Convention, Amsterdam, Convention Paper 5320*, 2001.

[42] D. Doldi, M. Mocellin, P. Antinori, R. Orsoni, G. Santarelli, M. Di Cola, and R. Grifoni, "Analysis and Minimization of Unwanted Resonances in Loudspeaker Systems via FEM Techniques," in *116th AES Convention, Berlin, Convention Paper 6099*, 2004.

[43] P. Larsen, "Geometrical Stiffness of Loudspeaker Cones," in *116th AES Convention, Berlin, Convention Paper 6095*, 2004.

[44] E. Prokofieva, "Radiation of Enclosed Loudspeaker in a Large Baffle: Speaker Simulation Model," in *116th AES Convention, Berlin, Convention Paper 6194*, 2004.

[45] Y. Kagawa, N. Kyouno, T. Usagawa, and T. Yamabuchi, "Acoustic Response Simulation of a Cone-Type Loudspeaker by the Finite Element Method," in *117th AES Convention, San Francisco, Convention Paper 6242*, 2004.

[46] T. Kärkkäinen Leo; Mellow, "On the Sound Field of a Membrane in an Infinite Baffle," in *118th AES Convention, Barcelona, Convention Paper 6419*, 2005.

[47] A. Salvatti, "Virtual Acoustic Prototyping, Practical Applications for Loudspeaker Development," in *129th AES Convention, San Fransisco, Convention Paper 8213*, 2010.

[48] M. Cobianchi and R. Magalotti, "Optimization of an Acoustic Waveguide for Professional Audio Applications," in *Excerpt from the Proceedings of the COMSOL Conference 2009 Milan*, 2009.

[49] D. J. Murphy and R. Morgans, "Modelling Compression Drivers using T Matrices and Finite Element Analysis," in *119th AES Convention, New York, Convention Paper 6580*, 2005.

[50] D. J. Murphy and R. Morgans, "Modelling Acoustic Horns with FEA," in *128th AES Convention, London, Convention Paper 8076*, 2010.

[51] A. Voishvillo, "Simulation of Horn Driver Response by Combination of Matrix Analysis and FEA," in *129th AES Convention, San Fransisco, Convention Paper 8214*, 2010.

[52] M. Hedges and Y. Lam, "Accuracy of Fully Coupled Loudspeaker Simulation Using COMSOL," in *Proceedings of the COMSOL Conference 2009 Milan*, COMSOL Multiphysics, 2009.

[53] M. Jones, L. Binks, and D. Henwood, "Finite element methods applied to the analysis of high-fidelity loudspeaker transducers," *Computers & Structures*, vol. 44, pp. 765–772, Aug. 1992.

[54] M. Dodd, "The Development of a Forward Radiating Compression Driver by the Application of Acoustic, Magnetic and Thermal Finite Element Methods," in *115th AES Convention, New York, Convention Paper 5886*, 2003.

[55] C. I. Beltran, "Calculated Response of a Compression Driver Using a Coupled Field Finite Element Analysis," in *105th AES Convention, San Francisco, Convention Paper 4748*, 1998.

[56] D. J. Henwood, "The Boundary Element Method and Horn Design," *J. Audio Eng. Soc.*, vol. 41, no. 6, pp. 485–496, 1993.

[57] J. Wright, "Finite Element Analysis As A Loudspeaker Design Tool," in *13th UK AES Conference: Microphones & Loudspeakers, Paper nr. 1670*, pp. 75–78, 1998.

[58] D. Henwood and G. Geaves, "Finite Element Modelling of a Loudspeaker Part 2: Applications," in *119th AES Convention, New York, Convention Paper 6593*, 2005.

[59] M. Opitz and R. Barnert, "Modern Development Tools for Dynamic Transducers," in *111th AES Convention, New York, Convention Paper 5438*, 2001.

[60] D. Biba and M. Opitz, "Convention Paper 7103 Headphones Model," *122nd AES Convention, Vienna, Convention Paper 7103*, 2007.

[61] P. Anthony and J. R. Wright, "Finite Element Analysis in the Design of High-Quality Loudspeakers," in *108th AES Convention, Paris, Convention Paper 5162*, 2000.

[62] P. C. Macey, *Acoustic and Structure Meracfion Problems using Finite and Boundary Nements*. Ph.d. thesis, Nottingham University, 1987.

[63] J. R. Wright, "Radiation impedance Calculafion by Finite Element Analysis," *Inst. Acoust. Bulletin*, vol. 19, no. 6, 1994.

[64] M. Petyt, *lntroducfion to Finite Element Vibration Analysis*. Cambridge: Cambridge Univ. Press, 1990.

[65] V. Dickason, *Loudspeaker Design Cookbook*. Peterborough, New Hampshire: Audio Amateur Press, 7th ed., 2006.

[66] J. F. Novak, "Performance of enclosures for low resonance high compliance loudspeakers," *J. Audio Eng. Soc.*, vol. 7, pp. 29–37, Jan. 1959.

[67] N. Thiele, "Loudspeakers in Vented Boxes: Part 1," *J. Audio Eng. Soc*, vol. 19, no. 5, pp. 382–392, 1971.

[68] N. Thiele, "Loudspeakers in Vented Boxes: Part 2," *J. Audio Eng. Soc*, vol. 19, no. 6, pp. 471–483, 1971.

[69] R. H. Small, "Closed-Box Loudspeaker Systems-Part 1: Analysis," *J. Audio Eng. Soc*, vol. 20, no. 10, pp. 798–808, 1972.

[70] D. J. Murphy, "Axisymmetric Model of a Moving-Coil Loudspeaker," *J. Audio Eng. Soc.*, vol. 41, no. 9, pp. 679–90, 1993.

[71] T. Shindo, O. Yashima, and H. Suzuki, "Effect of Voice-Coil and Surround on Vibration and Sound Pressure Response of Loudspeaker Cones," *J. Audio Eng. Soc*, vol. 28, no. 7/8, pp. 490–499, 1980.

[72] K. Suzuki and I. Nomoto, "Computerized Analysis and Observation of the Vibration Modes of a Loudspeaker Cone," *J. Audio Eng. Soc.*, vol. 30, no. 3, pp. 98–106, 1982.

[73] C. J. Struck, "Analysis of the Nonrigid Behavior of a Loudspeaker Diaphram Using Modal Analysis," in *J. Audio Eng. Soc.*, vol. 38, pp. 667–675, 1989.

[74] COMSOL, "Tutorial model: Loudspeaker driver," 2010.

[75] S. Kirkup, *The Boundary Element Method in Acoustics*. Integrated Sound Software, 1998.

[76] J. W. S. Rayleigh, *The Theory of Sound, vol. 2*. New York: 1896; reprinted by Dover, 1945.

[77] H. Denli, S. Frangakis, and J. Q. Sun, "Normalizations in acoustic optimization with Rayleigh integral," *Journal of Sound and Vibration*, vol. 284, no. 3-5, pp. 1229–1238, 2005.

[78] S. Kirkupp, "Boundary Element Method in Acoustics." `http://www.boundary-element-method.com/acoustics`, 1. June 2011.

[79] J. D'Appolito, "Testing Loudspeakers: Which Measurements Matter, Part 2," *audioXpress*, vol. Oct., pp. 28–36, 2009.

[80] B. Kolbrek, "Horn Theory: An Introduction, Part 1," *audioXpress*, no. 3, p. 6, 2008.

[81] B. Kolbrek, "Horn Theory: An Introduction, Part 2," *audioXpress*, no. 3, p. 20, 2008.

[82] J. Holm, *Applying the Finite Element Method for Modelling Loudspeaker Waveguide Directivity*. Master thesis, Aalto University, Finland, 2010.

[83] COMSOL, "COMSOL Multiphysics User's Guide 4.1," Sept. 2010.

[84] M. B. Drozdz, *Efficient finite element modelling of ultrasound in elastic media*. Ph.d thesis, Imperial college of science technology and medicine, University of London, 2008.

[85] SEAS Website. `http://www.seas.no/index.php?option=com_content&task=view&id=179&Itemid=174`, 1. June 2011.

[86] COMSOL, "Acoustics Module User's Guide 4.1," 2010.

[87] N. Kyouno, "Acoustic Radiation of a Horn Loudspeaker by the Finite Element Method-Acoustic Characteristics of a Horn Loudspeaker with an Elastic Diaphragm," 1982.

[88] E. Wente, "Acoustic Device," *US patent 1930915*, p. issued 17. Oct., 1933.

[89] COMSOL, "LiveLink for MATLAB User Guide," 2010.

[90] R. C. Morgans, A. C. Zander, C. H. Hansen, and D. J. Murphy, "EGO shape optimization of horn-loaded loudspeakers," *Optimization and Engineering*, vol. 9, pp. 361–374, Nov. 2008.

[91] E. Bengtsson, D. Noreland, and M. Berggren, "Shape optimization of an acoustic horn," *Computer Methods in Applied Mechanics and Engineering*, vol. 192, pp. 1533–1571, Mar. 2003.

[92] G. Miccoli, "Vibroacoustic optimization of loudspeaker components," in *Sixth International Congress on Sound and Vibration*, pp. 625–634, 1999.

[93] S. Christensen and N. Ohloff, "Shape optimization of a loudspeaker diaphragm with respect to sound directivity properties," *Control and Cybernetics*, vol. 27, no. 2, pp. 177–198, 1998.

[94] S. T. Christensen, S. V. Sorokin, and N. Olhoff, "On analysis and optimization in structural acoustics-Part I: Problem formulation and solution techniques," *Structural and Multidisciplinary Optimization*, vol. 16, no. 2-3, pp. 83–95, 1998.

[95] S. T. Christensen, S. V. Sorokin, and N. Olhoff, "On analysis and optimization in structural acoustics-Part II:Exemplifications for axisymmetric structures," *Structural and Multidisciplinary Optimization*, vol. 16, no. 2-3, pp. 96–107, 1998.

[96] P. Macey, "Cone Shape Optimization based on FE/BE Simulation to Improve the Radiated Sound Fiels," in *127th AES Convention, New York, Convention Paper 7836*, 2009.

[97] D. Noreland and R. Udawalpola, "An efficient loudspeaker horn designed by numerical optimization: an experimental study," *Unpublished report, UmeåUniversity, Sweden*, 2010.

[98] G. P. Geaves, "Design and Validation of a System for Selecting Optimized Midrange Loudspeaker Diaphragm Profiles," *J. Audio Eng. Soc*, vol. 44, no. 3, pp. 107–118, 1996.

[99] R. E. Steuer, *Multiple Criteria Optimization: Theory, Computations, and Application*. New York: John Wiley & Sons, Inc, 1986.

[100] Y. Sawaragi, H. Nakayama, and T. Tanino, *Theory of Multiobjective Optimization*. Orlando: Academic Press Inc., 1985.

[101] Chris Lucas, "Practical Multiobjective Optimisation." `http://www.calresco.org/lucas/pmo.htm`, 1. June 2011.

[102] COMSOL, "Tutorial model: Optimizing the Shape of a Horn," 2010.

[103] M. S. Ureda, "On the Movement of a Horns Acoustic Center," in *106th AES Convention, Munich, Convention Paper 4986*, 1999.

[104] J. Vanderkooy, "Applications of the Acoustic Centre," in *122nd AES Convention, Vienna, Convention Paper 7102*, 2007.

[105] P. Macey, "Accuracy issues in finite element simulation of loudspeakers," in *125th AES Convention, San Fransico, Convention Paper 7600*, 2008.

[106] IEEE Spectrum Online Webinar, "Acoustics simulation in microphones, mobile devices and hearing aids using COMSOL." `http://event.on24.com/eventRegistration/prereg/register.jsp?eventid=313093&sessionid=1&key=FA1F4A2E6CAB1ECA9BFEA7CD24308A45`, 15. June 2011.

Appendix A

Driver Specifications

SEAS PRESTIGE

27TFFC H0881

27TFFC is a High Fidelity precoated fabric dome tweeter with an integral wide surround and a rear chamber.

Sonolex precoated lightweight fabric diaphragm with high consistency and excellent stability against variations in air humidity.

Voice coil windings immersed in magnetic fluid increase short term power handling capacity and reduce the compression at high power levels.

Stiff and stable rear chamber with optimal acoustic damping allows the tweeter to be used with moderately low crossover frequencies.

The chassis is precision moulded from glass fibre reinforced plastic, and its front design offers optimum radiation conditions.

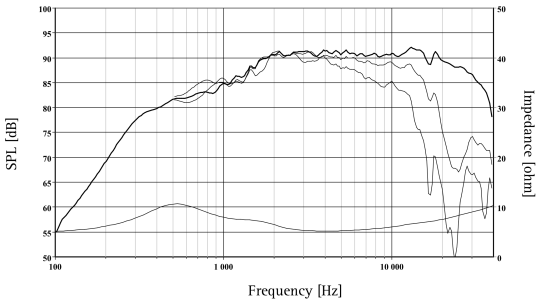

The frequency responses above show measured free field sound pressure in 0, 30, and 60 degrees, mounted in a 0.6m by 0.8m baffle. Input 2.83 Vrms, microphone distance 0.5m, normalized to SPL 1m. The impedance is measured without baffle using a 2V sine signal.

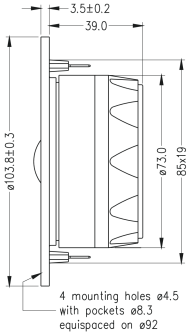

Nominal Impedance	6 Ohms	Voice Coil Resistance	4.8 Ohms
Recommended Frequency Range	2000 - 30000 Hz	Voice Coil Inductance	0.05 mH
Short Term Power Handling *	200 W	Force Factor	3.5 N/A
Long Term Power Handling *	80 W	Free Air Resonance	550 Hz
Characteristic Sensitivity (2.83V, 1m)	91 dB	Moving Mass	0.25 g
Voice Coil Diameter	26 mm	Effective Piston Area	7.6 cm^2
Voice Coil Height	1.5 mm	Magnetic Gap Flux Density	1.8 T
Air Gap Height	2.0 mm	Magnet Weight	0.25 kg
Linear Coil Travel (p-p)	0.5 mm	Total Weight	0.52 kg

Jul 2007-1 *IEC 268-5, via High Pass Butterworth Filter 2500Hz 12 dB/oct. T27-701

SEAS reserves the right to change technical data

SEAS PRESTIGE

27TBCD/GB-DXT H1499

DXT® DIFFRACTION EXPANSION TECHNOLOGY

27TBCD/GB-DXT is a High Definition aluminium/magnesium alloy dome tweeter with DXT® lens.

An optimally shaped dome and a wide SONOMEX surround, both maufactured by SEAS, ensure excellent performance and consistency.

The compensation magnet increases the sensitivity and reduces the magnetic strayfield and allows use in close proximity to CRT screens.

A fine mesh grid protects the diaphragm.

Stiff and stable rear chamber with optimal acoustic damping allows the tweeter to be
used with moderately low crossover frequencies.

This revolutionary DXT® tweeter addresses the major issues regarding directivity control in traditional loudspeaker designs. DXT® solves several well-know issues regarding; directivity control, off-axis response, integration with midrange units and baffle diffractions.

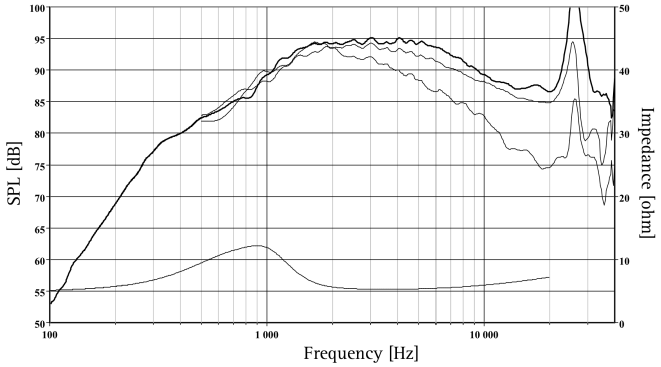

The frequency responses above show measured free field sound pressure in 0, 30, and 60 degrees, mounted in a 0.6m by 0.8m baffle. Input 2.83 Vrms, microphone distance 0.5m, normalized to SPL 1m. The impedance is measured without baffle using a 2V sine signal.

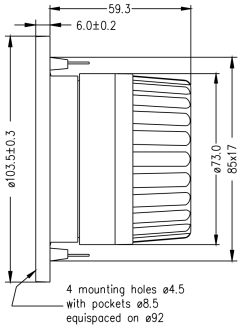

Nominal Impedance	6 Ohms	Voice Coil Resistance	4.8 Ohms
Recommended Frequency Range	2000 - 25000 Hz	Voice Coil Inductance	0.05 mH
Short Term Power Handling *	150 W	Force Factor	3.7 N/A
Long Term Power Handling *	55 W	Free Air Resonance	900 Hz
Characteristic Sensitivity (2.83V, 1m)	92.0 dB	Moving Mass	0.33 g
Voice Coil Diameter	26 mm	Effective Piston Area	7.5 cm^2
Voice Coil Height	1.5 mm	Magnetic Gap Flux Density	1.9 T
Air Gap Height	2.0 mm	Magnet Weight	0.35 kg
Linear Coil Travel (p-p)	0.5 mm	Total Weight	0.64 kg

Oct 2007-1

*IEC 268-5, via High Pass Butterworth Filter 2500Hz 12 dB/oct.
SEAS reserves the right to change technical data

T27-951

Appendix B

Example script, COMSOL LiveLink for MATLAB

```
clear all
close all
clc
%Add search path for COMSOL model file
path(path,'/Users/COMSOL_MASTER')

disp(['Loading COMSOL model...'])
disp(' ')
%Load COMSOL model
model = mphload('tweeterModel.mph');

% Geometric parameters (initial conditions)
dummyVariable= 0;
topCenterZ =28;
legCenterR =4;
legCenterZ =6;
topRightR =18.0;
topRightZ =20.0;
leftLegR =6;
leftLegZ =6;
rightLegR =13;
rightLegZ =1.8;
middleCenterZ=5.5;

numberOfGeometrySweeps=100;

 for i=1:numberOfGeometrySweeps;

disp(['Starting geometry ' num2str(i) ' and randomizing ...
```

```
    gemometry vertices...'])
disp(' ')

% While loop generated random geometry vertices until a ...
    valid one is found
notValid=1;
   while notValid

    %Randomizing vertices within a given geometric search range:
    topCenterZA=30;
    topCenterZB=40;
    topCenterZ =topCenterZA + (topCenterZB-topCenterZA) * ...
       rand();

    legCenterRA=2;
    legCenterRB=3;
    legCenterR =legCenterRA + (legCenterRB-legCenterRA) * ...
       rand();

    legCenterZA=9;
    legCenterZB=11;
    legCenterZ =legCenterZA + (legCenterZB-legCenterZA) * ...
       rand();

    topRightRA=25;
    topRightRB=40;
    topRightR =topRightRA + (topRightRB-topRightRA) * rand();

    topRightZA=20;
    topRightZB=30;
    topRightZ =topRightZA + (topRightZB-topRightZA) * rand();

    leftLegRA=8;
    leftLegRB=11;
    leftLegR =leftLegRA + (leftLegRB-leftLegRA) * rand();

    leftLegZA=4;
    leftLegZB=8;
    leftLegZ =leftLegZA + (leftLegZB-leftLegZA) * rand();

    rightLegRA=12;
    rightLegRB=15;
    rightLegR =rightLegRA + (rightLegRB-rightLegRA) * rand();

    rightLegZA=1;
    rightLegZB=4;
    rightLegZ =rightLegZA + (rightLegZB-rightLegZA) * rand();

    middleCenterZA=5;
```

```
    middleCenterZB=6;
    middleCenterZ =middleCenterZA + ...
        (middleCenterZB-middleCenterZA) * rand();

%   Checking if point is above a diagonal line, in order to ...
   reduce search
%   space further
%    upper line range (25, 20) to ( 42, 36)
%    lower line range (26, 18) to (42, 28)

    X=[25 42];
    Y=[20 36];
    % dYI is the distance from the curve
    dYI=interp1(X,Y,topRightR,'linear')-topRightZ;
    %-->dYI negative  means that the point is over the line
    X2=[26 42];
    Y2=[18 28];
    % dYI is the distance from the curve
    dYI2=interp1(X2,Y2,topRightR,'linear')-topRightZ;

    notValid=0;

            if (dYI<0) || (dYI2>0)
                 disp('Invalid Geometry, but remaking ...
                    geometry !!!!!!!!!!!!!!!!')
            notValid=1;
            end

    end % End while and finished randomizing and geometry check


disp('Displaying geometry...')
disp(' ')
%Display geometry
figure(1)
hold on
plot([0 legCenterR], [middleCenterZ legCenterZ])
plot([legCenterR 0], [legCenterZ topCenterZ])
plot([leftLegR rightLegR], [leftLegZ rightLegZ])
plot([rightLegR topRightR], [rightLegZ topRightZ])
plot([topRightR leftLegR], [topRightZ leftLegZ ])
xlim([-5 70])
ylim([-10 70])
axis square
% Save geometry plot to file:
fileName= ['Geometries_Iterated.png'];
saveas(gcf, fileName)
hold off
```

```
%--------------------------------
% Assembling parameter string for COMSOL:
parameterizationString= [num2str(dummyVariable) ...
    ' ' num2str(topCenterZ) ' ' num2str(legCenterR) ' ' ...
       num2str(legCenterZ) ...
    ' ' num2str(topRightR) ' ' num2str(topRightZ) ...
   ' ' num2str(leftLegR) ' ' num2str(leftLegZ) ...
   ' ' num2str(rightLegR) ' ' num2str(rightLegZ) ...
   ' ' num2str(middleCenterZ)];

%Performing FEA in COMSOL
disp('Performing FEA in COMSOL...')
disp(' ')

% Setting geometric parameters:
model.study('std2').feature('param').set('plist', ...
   parameterizationString);
%Running study
model.batch('p1').run;


disp('Retrieving data from COMSOL...')
disp(' ')
% Retrieving data from calculated COMSOL model
pointNr=11; %Comsol evaluation point on-axis
outerSolNum=1;
sensitivity_0 = ...
   mpheval(model,'SPL','dataset','dset5','edim',0,'selection',pointNr, ...
   'Outersolnum', outerSolNum);
sensitivity_075 = ...
   mpheval(model,'SPL075','dataset','dset5','edim',0,'selection',pointNr, ...
   'Outersolnum', outerSolNum);
sensitivity_15 = ...
   mpheval(model,'SPL15','dataset','dset5','edim',0,'selection',pointNr, ...
   'Outersolnum', outerSolNum);
sensitivity_225 = ...
   mpheval(model,'SPL225','dataset','dset5','edim',0,'selection',pointNr, ...
   'Outersolnum', outerSolNum);
sensitivity_30 = ...
   mpheval(model,'SPL30','dataset','dset5','edim',0,'selection',pointNr, ...
   'Outersolnum', outerSolNum);
sensitivity_375 = ...
   mpheval(model,'SPL375','dataset','dset5','edim',0,'selection',pointNr, ...
   'Outersolnum', outerSolNum);
sensitivity_45 = ...
   mpheval(model,'SPL45','dataset','dset5','edim',0,'selection',pointNr, ...
   'Outersolnum', outerSolNum);
sensitivity_525 = ...
   mpheval(model,'SPL525','dataset','dset5','edim',0,'selection',pointNr, ...
```

```
    'Outersolnum', outerSolNum);
sensitivity_60 = ...
    mpheval(model,'SPL60','dataset','dset5','edim',0,'selection',pointNr, ...
    'Outersolnum', outerSolNum);
freq= mpheval(model,'freq','dataset','dset5', ...
    'edim',0,'selection',pointNr, 'Outersolnum', outerSolNum);
%--------------------------------

disp('Plotting...')
disp(' ')
%Insert relevant MATLAB code for plotting here

disp('Displaying COMSOL geometry...')
disp(' ')
%Display geometry:
figure(2)
mphgeom(model,'geom1','vertexmode','on', 'edgemode','on')
axis square
% Save geometry to file:
fileName= ['ComsolPlot_GeometryNr' num2str(i) '.png'];
saveas(gcf, fileName)


% Preparing Geometry Goodness Plots:
relativeResponse6kHz(i)= ...
    (sensitivity_60.d1(9)-sensitivity_0.d1(9));
relativeResponse8kHz(i)= ...
    (sensitivity_60.d1(14)-sensitivity_0.d1(14));
relativeResponse10kHz(i)= ...
    (sensitivity_60.d1(18)-sensitivity_0.d1(18));
relativeResponse11_8kHz(i)= ...
    (sensitivity_60.d1(21)-sensitivity_0.d1(21));
relativeResponse14kHz(i)= ...
    (sensitivity_60.d1(24)-sensitivity_0.d1(24));


%Standard deviation of entire relative response:
stdRelativeresponse_allfreq(i)= ...
    std(sensitivity_60.d1-sensitivity_0.d1);

%Standard deviation of relative response in frequency range ...
    1.7-15kHz:
stdRelativeresponse_smallerRange(i)= ...
    std(sensitivity_60.d1(2:25)-sensitivity_0.d1(2:25));


%Sum over all angles, Standard deviation of relative
% response in frequency range 1.7-15kHz:
stdSumAllAnglesRelativeresponse_smallerRange(i)= ...
```

```
    std(sensitivity_075.d1(2:25)-sensitivity_0.d1(2:25))...
    +std(sensitivity_15.d1(2:25)-sensitivity_0.d1(2:25))...
    +std(sensitivity_225.d1(2:25)-sensitivity_0.d1(2:25))...
    +std(sensitivity_30.d1(2:25)-sensitivity_0.d1(2:25))...
    +std(sensitivity_375.d1(2:25)-sensitivity_0.d1(2:25))...
    +std(sensitivity_45.d1(2:25)-sensitivity_0.d1(2:25))...
    +std(sensitivity_525.d1(2:25)-sensitivity_0.d1(2:25))...
    +std(sensitivity_60.d1(2:25)-sensitivity_0.d1(2:25));

disp(['Sorting geometry' num2str(i) '..... '])
disp(' ')
%Insert code here for sorting geometries by performance in ...
   as many
%categories as the objectieve evaluation functions allow.

disp(['Discarding geometry' num2str(i) '..... '])
disp(' ')
discardingThreshold= 50; %
% Discard geometries below a certain threshold
if ...
    stdSumAllAnglesRelativeresponse_smallerRange(i)>discardingThreshold
% Insert discarding code
end

disp(['Saving workspace' num2str(i) '..... '])
disp(' ')
% Saving workspace to file related to geometry number:
fileName= ...
    ['MatlabSweepResults/Workspace/workSpace_GeometryNr' ...
    num2str(i)];
save(fileName);

disp(['End geometry ' num2str(i) '. '])
disp(' ')
 end % end COMSOL for-loop

disp(['Finished!!!!!!!!!!!!!'])
disp(' ')
 %-----------------------------------------------------------------------
```

Appendix C

Appended DVD

The appended DVD includes:

- Animations of wave propagation
- Measurement plots
- Comsol model files with solution
- CAD files
- Solutions from geometry sweeps
- Matlab code
- Driver specifications